

ROTATIONAL VELOCITY OF THE METAL-POOR K-GIANT STARS IN THE MILKY WAY

A Project Work

Submitted to the Department of Physics,
Tri-Chandra Multiple Campus,in the Partial Fulfillment for the
Requirement of Bachelor's Degree of Science in Physics



By

Ukesh Karki

TU Reg no.: 5 - 2 - 37 - 840 - 2016

Symbol no.: 371357

February, 2021



Declaration

Project report entitled **Rotational Velocity of the Metal-Poor K-giant Stars in the Milky Way** which is being submitted to the Department of Physics Tri-Chandra Multiple Campus, is a project work carried out by me under the supervision of Asst. Prof. Madhu Sudan Paudel and Mr. Raj K Pradhan.

I hereby declare that this written submission represents my ideas in my own words and where other's ideas or words have been included and I have cited the references of the original sources that I have used.

Mr. Ukech Karki
B.Sc. 4th year
TU Reg no.: 5 - 2 - 37 - 840 - 2016
Symbol no.: 371357
Department of Physics
Tri-Chandra Multiple Campus
Ghantaghar, Kathmandu, Nepal

Date:.....



Recommendation

It is certified that **Mr. Ukesh Karki** has carried out the project work entitled **Rotational Velocity of the Metal-Poor K-giant Stars in the Milky Way** under my supervision.

I recommend the project work in the Partial fulfillment for the requirement of Bachelor's Degree of Science in Physics.

Asst. Prof. Madhu Sudan Paudel
Supervisor
Department of Physics
Tri-Chandra Campus
Ghantaghari, Kathmandu, Nepal

Raj Kumar Pradhan
Co-supervisor
Department of Physics
Amrit Campus
Thamel, Kathmandu, Nepal
Pokhara Astronomical Society

Date:.....

Acknowledgements

I would like to express my deepest gratitude to my supervisors, **Asst. Prof. Madhu Sudan Paudel** and **Raj K Pradhan** for their eternal support, dedication, guidance, and patience and also for giving me the opportunity to learn fundamentals to advanced skills either theory or programming. Under their supervision, I got exposure to the entirely new paradigm of astrophysics to which I was unfamiliar before, learned the skills and knowledge that will last with me forever for my further physics career. I would be incomplete if I say my supervisors taught me only astrophysics. They taught me what it meant to be honest, hard-working, passionate, and dedicated. In some sense, they made me a better person and they increased my love for astrophysics.

I would like to thank my brother **Umesh Karki** for exposing me to the world of computer programming especially, Python programming which ought to be very beneficial for my project work. He is a physicist himself who is also a source of my inspiration and always encouraged me to learn more fundamental physics.

I would like to express my gratitude to **Dr. Prajwal R. Kafle** (The University of Western Australia), Professor Jo Bovy (University of Toronto), Jason Hunt (Flatiron Institute) for their comments, suggestions, and help that have played a vital role in the completion of my project work.

I like to express my sincere gratitude to **Asst. Prof. Iswar Prasad Koirala**, Head of Department, Tri-Chandra Multiple Campus for his constant encouragement, suggestions, and support. And, I am also thankful for all faculty members of the Department of Physics, Tri-Chandra Multiple Campus.

My sincere thanks go to my friends Pranam Lama, Dip Khadka, Rashmi Adhikari, Ganesh Acharya, Kritinidhi Chimariya, and Galactic Dynamic group for their endless support for the completion of my project work.

I also like to acknowledge Gaia and GALAH for making their data accessible for our research and I am also grateful for Astropy and Galpy.

This research project would not have been possible without the continuous support, encouragement, and love of my parents. So, I like to thank them for everything.



Letter of Approval

We certify that we have read this project work and in our opinion it is good in the scope and quality as project work in the partial fulfillment for the requirement of Bachelor's Degree of Science in Physics.

External Examiner

Internal Examiner

Asst. Prof. Madhu Sudan Paudel
Supervisor

Asst. Prof. Iswar Prasad Koirala
Head
Department of Physics
Tri-Chandra Multiple Campus
Ghantaghari, Kathmandu, Nepal

Raj Kumar Pradhan
Co-supervisor

Date:.....



Certificate

This is to certify that the project report **Rotational Velocity of the Metal-Poor K-giant Stars in the Milky Way** carried out by Mr. Ukesh Karki, of final year B.Sc. in physics during the year 2020 – 2021 is an excellent work submitted to the Department of Physics, Tri-Chandra Multiple Campus, Tribhuvan University, Kathmandu, in partial fulfillment of requirement for the award of degree of Bachelor of Science in Physics.

Asst. Prof. Madhu Sudan Paudel
Supervisor
Department of Physics
Tri-Chandra Campus
Ghantaghari, Kathmandu, Nepal

Asst. Prof. Iswar Prasad Koirala
Head
Department of Physics
Tri-Chandra Campus
Ghantaghari, Kathmandu, Nepal

Raj Kumar Pradhan
Co-supervisor
Department of Physics
Amrit Campus
Thamel, Kathmandu, Nepal
& Pokhara Astronomical Society, Nepal

Date:.....

Acronyms

AJ : Astronomical Journal

ApJ : Astrophysical Journal

ApJS : Journal Suppliment

ARAA : Annual Review of Astronomy and Astrophysics

MNRAS : Monthly Notice of Royal Astronomical Society

MSTO : Main Sequence Turn – off

BHB : Blue Horizontal Branch

MCMC : Markov Chain Monte Carlo

GALAH : Galactic Archaeology with HERMES

EDR3 : Early Data Release3

MWTD : Metal Weak ThickDisk

List of Figures

2.1	Stellar parallax of star with parallax (p) situated at distance (d) from the Sun, where 1 AU (Astronomical Unit) is distance between the Sun and Earth.	9
2.2	Proper motion of the star.	10
2.3	H-R diagram, here we can see the position of stars divided according to temperature, spectral class, luminosity and absolute magnitude. [1]	14
2.4	Probability density function of the Gaussian distribution with mean μ and variance σ^2	16
3.1	Temperature versus logg plot for entire dataset of GALAH cross-matched with Gaia (represented by blue dot), K-giant stars in GALAH (represented by orange dot) and K-giant stars selected for our research (represented by green dot).	25
3.2	Mollweide projection of selected K-giant stars with the color bar representing there metallicity [Fe/H]	26
3.3	Spatial distribution of position of K-giant stars in Galactocentric cartesian coordinate system. Left panel: The distribution of K-giant stars in $z - x$ plane and at center of $z = 0.025$ kpc and $x = R_\odot$. Right panel: The distribution of K-giant stars in $y - x$ plane.	34

3.4	Distribution of velocity of the K-giant stars in Galactocentric cartesian coordinate system.	34
3.5	The galactocentric radius r_{gc} versus radial velocity V_r	35
3.6	The galactocentric radius r_{gc} versus polar velocity V_θ	35
3.7	The galactocentric radius r_{gc} versus azimuthal velocity V_ϕ	35
3.8	The metallicity [Fe/H] versus radial velocity V_r	36
3.9	The metallicity [Fe/H] versus polar velocity V_θ	36
3.10	The metallicity [Fe/H] versus azimuthal velocity V_ϕ	36
3.11	The distributions of the velocity of K-giant stars in a cylindrical coordinate system. Along the diagonal, the distribution of cylindrical velocity components in the histogram and in off-diagonal, the scattering plot between various cylindrical velocity-components.	37
3.12	The distributions of the velocity of K-giant stars in a spherical coordinate system. Along the diagonal, the distribution of spherical velocity components in the histogram and in off-diagonal, the scattering plot between various spherical velocity-components.	38
4.1	The plot of distribution of azimuthal velocity (V_T) with an error bar generated using Poisson distribution. The dark black line represents the entire sample, the red dash line represents the first component, the blue dash line represents the second component and the green dash line represents the third component.	41

4.2	The result of MCMC is shown in the corner plot. The corner plot shows the correlation between any two parameters. The blue line indicates the median value of samples which we have taken as the best fit. 1σ , 2σ and 3σ contours shows the joint posterior probability distribution of our parameters (θ_i 's) for K-giant stars. The histogram represents one-dimensional marginalized posterior distribution.	42
4.3	Position of our walker as a function of the number of steps (for all 3081 K-giant stars). This plot also depicts more about walkers having entire parameter space of posterior distribution. This plot represents the random walk followed by the walkers.	43
4.4	The plot of velocity anisotropy(β) as a function of the galactocentric radius, here we have binned star at 2.5 kpc galactocentric radius.	44
4.5	Plot of the velocity dispersions ($\sigma_r, \sigma_\theta, \sigma_\phi$) with the galactocentric radius binned at 2.5 kpc.	44
4.6	Plot of velocity anisotropy (β) as a function of the metallicity ([Fe/H]). Here we have binned the star in 0.3 dex metallicity. 45	45
4.7	Energy vs total angular momentum plot of our 3081 K-giant stars where potential is evaluated using McMillian17 of galpy. [23].	46
4.8	Energy vs z-component of angular momentum plot of our 3081 K-giant stars where potential is evaluated using McMillian17 of galpy. [23].	47

- 4.9 The result of MCMC for K-giant stars with metallicity $-0.9 \text{ dex} < [\text{Fe}/\text{H}] < -0.5 \text{ dex}$ is shown in the corner plot. Corner plot shows the correlation between any two parameters. The blue line indicate the median value of samples which we have taken as a best fit. 1σ , 2σ and 3σ contours shows the joint posterior probability distribution of our parameters (θ_i 's) for K-giant stars. The histogram represent one dimensional marginalize posterior distribution. 48
- 4.10 Position of our walkers as a function of number of steps (for all K-giant stars with metallicity $-0.9 \text{ dex} < [\text{Fe}/\text{H}] < -0.5 \text{ dex}$). 49
- 4.11 The result of MCMC for K-giant stars with metallicity $-1.3 \text{ dex} < [\text{Fe}/\text{H}] < -0.9 \text{ dex}$ is shown in the corner plot. Corner plot shows the correlation between any two parameters. The blue line indicate the median value of samples which we have taken as a best fit. 1σ , 2σ and 3σ contours shows the joint posterior probability distribution of our parameters (θ_i 's) for K-giant stars. The histogram represent one dimensional marginalized posterior distribution. 50
- 4.12 Position of our walkers as a function of number of steps (for all K-giant stars with metallicity $-1.3 \text{ dex} < [\text{Fe}/\text{H}] < -0.9 \text{ dex}$). 51

4.13 The result of MCMC for K-giant stars with metllicity – 2.5 dex < [Fe/H] < – 1.3 dex is shown in the corner plot. Corner plot shows the correlation between any two parameters. The blue line indicate the median value of samples which we have taken as a best fit. 1σ , 2σ and 3σ counters shows the joint posterior probability distribution of our parameters (θ_i 's) for K-giant stars. The histogram represent one dimensional marginalize posterior distribution.	52
4.14 Position of our walkers as a function of number of steps (for all K-giant stars halo stars with metallicity – 2.5 dex < [Fe/H] < – 1.3 dex).	53
4.15 Distribution of the azimuthal velocity V_T of 3081 K-giant stars divided according to metallicity, first being the metal richest and third being the metal poorest K-giant stars in our sample. Here error is generated using the Poisson distribution.	54
4.16 Energy versus angular momentum plot obtained by Bird <i>et al.</i> (2018) [8]	56

List of Tables

4.1	Source id, right ascension, declination, parallax, proper motions, radial velocity, energy, angular momentum and angular momentum along z - direction for 10 K-giant stars out of 3081 K-giant stars on our data.	46
4.2	Table shows the results of MCMC simulation for different K-giant stars grouping that we made.	56

List of Symbols

M_\odot	Mass of the Sun	kg
L_\odot	Luminosity of the sun	$J\ s^{-1}$
R_\odot	Distance of Sun from the galactic center	kpc
$U_\odot, V_\odot, W_\odot$	Velocity of the Sun in 3 dimension	$km\ s^{-1}$
α	Right ascension	deg
δ	Declination	deg
l	Galactic longitude	deg
b	Galactic latitude	deg
μ_α	Proper motion along right ascension	$mas\ yr^{-1}$
μ_δ	Proper motion along declination	$mas\ yr^{-1}$
μ_l	Proper motion along galactic longitude	$mas\ yr^{-1}$
μ_b	Proper motion along galactic latitude	$mas\ yr^{-1}$
\bar{w}	Parallax	mas
σ_r	Radial velocity dispersion	$km\ s^{-1}$
σ_θ	Rotational velocity dispersion	$km\ s^{-1}$
σ_ϕ	Azimuthal velocity dispersion	$km\ s^{-1}$

Abstract

With the release of the Gaia EDR3 better estimation of parallax is available which was crossmatched with GALAH DR3 for full 6-dimensional phase space information. 3081 K-giant with $[\text{Fe}/\text{H}] < -0.5$ are taken within the 4 kpc to 12 kpc whose rotational velocity is fitted to three Gaussian components. In which one component represent the halo and shows the rotational velocity of $V_T = -5^{+3}_{-3}$ km s $^{-1}$ with dispersion of $\sigma_T = 55^{+3}_{-3}$ km s $^{-1}$ that exhibits the retrograde motion. With metallicity ($-0.9 < [\text{Fe}/\text{H}] < -0.5$), metal-rich K-giants show prograde motion while metal-poor K-giant stars with metallicity ($[\text{Fe}/\text{H}] < -0.9$) shows retrograde motion. But the variation in velocity with metallicity is significantly small. This result indicates the weak correlation of rotational velocity with metallicity. Along with halo component we find the small fraction of metal weak thick disk which has rotational velocity $V_T = 134^{+16}_{-16}$ km s $^{-1}$ with dispersion of $\sigma_T = 59^{+12}_{-12}$ km s $^{-1}$, and another fraction of outer halo with velocity $V_T = -41^{+19}_{-19}$ km s $^{-1}$ that has a dispersion of $\sigma_T = 153^{+7}_{-7}$ km s $^{-1}$. Also, we estimate the velocity anisotropy of the K-giant sub-samples where we find the value of $\beta = 0.48$ that indicates the radially biased orbit for K-giant stars.

Contents

Declaration	i
Recommendation	ii
Acknowledgements	iii
Letter of Approval	iv
Certificate	v
Acronyms	vi
List of Figures	vii
List of Tables	xii
List of Symbols	xiii
Abstract	xiv
1 Introduction	1
1.1 Milky Way	2
1.1.1 The Thin Disk	2
1.1.2 The Thick Disk	3
1.1.3 The Bulge	3
1.1.4 The Galactic Halo	4

1.2	Motivation	4
1.3	Objective	6
1.4	Significance of the Study	6
1.5	Limitations of the Study	7
2	Theory	8
2.1	Parallax	8
2.2	Proper Motion	9
2.3	Velocity Anisotropy	10
2.4	Metallicity	13
2.5	K-giant	14
2.6	Gaussian Distribution	15
2.7	Bayes' Theorem	16
2.8	Markov Chain Monte Carlo (MCMC)	17
2.9	Energy and Angular Momentum	19
2.10	Gaia	21
2.11	GALACTIC Archaeology with HERMES (Galah)	22
3	Data & Method	23
3.1	Data	23
3.2	Method	27
3.2.1	Transformation of Coordinates and Velocity	27
3.2.2	Relationship between the Cartesian Coordinate, Spherical Coordinate and Cylindrical Coordinate	29
3.2.3	Determination of Rotational Velocity	31
3.2.4	Determination of Velocity Anisotropy (β)	32
4	Result & Discussion	39
4.1	Result	39
4.1.1	Rotational Velocity	39

4.1.2 Velocity Anisotropy	44
4.1.3 Energy and Angular Momentum	45
4.2 Discussion	48
5 Conclusions & Future Works	58
5.1 Conclusion	58
5.2 Future Works	59
References	60

Chapter 1

Introduction

Galaxy is complex system that is bounded together with different component like stars, stellar remnants, interstellar gas and majorly with dark matter. Distance between galaxies is increasing as the universe is expanding continuously. Galaxy is divided into 3 general types according to their morphology as elliptical, spiral, irregular. Research has revealed that there are trillions of galaxies in the universe. Many galaxies are believed to have supermassive black holes in their centers. Space in between galaxies is not empty but is filled with one atom per meter cube. The Galaxy consists of a massive number of stars ranging from a few hundred million in dwarf galaxies to one hundred trillion in giant galaxies.

Observational measurement of stars in space is termed referred as stellar kinematics. In other words, it is simply the study of the motion of a star in space. Studying the kinematics of stars in a different region of the Milky Way (i.e bulge, disk, halo) enables us to understand the history of the galaxies. This kind of study also helps us to determine the hypervelocity star that is capable of escaping the Milky Way galaxy. Here we also define the model in order to construct the astrophysical system.

Measurement of velocity of stars in the innermost region of galaxies has given evidence that most of the galaxies hold a black hole at a centre.

1.1 Milky Way

Milky Way is a barred spiral galaxy with 100 - 400 billion stars. In the early 17th century Galileo Galilei discovered that Milky Way consists of a large number of stars. Later William Herschel tried to determine the size and shape of the Milky Way but it was only in the 20th century Jacobus Kapteyn obtain the first estimate of the size of the Milky Way. Later in 1990's Harlow Shapley studied the space distribution of Globular clusters and found the true size of the Milky Way galaxy as well as position of the Sun in the Milky Way. [1].

The main component of the Milky Way is disk, bulge, halo. Further, the disk is divided into the thin disk and the thick disk, the halo is divided into the stellar halo, and the dark matter halo. [2].

1.1.1 The Thin Disk

According to nucleocosmochronology, the thin disk of the Milky Way which have been formed around 8.8 ± 1.7 billion years ago [3]. The thin disk is younger than the thick disk. The majority of stars in the Solar neighborhood are in a thin disk. It has a wide range of age of stars from younger to older, the older star which found in it is about 8 ± 1.5 Gyr [2]. These star along with dust and gases follows exponential distribution approximately along both radial and z-direction. The thin disk rotates rapidly with a circular velocity at Solar radius 215 ± 20 km s⁻¹ [2].

1.1.2 The Thick Disk

The thick disk is a source of kinematic and chemical evidence for galaxy's composition, so it is regarded as an important asset to study galaxy formation. As a thick disk is older and metal-poor compared to a thin disk, it contains information about the early stages of the galaxy. The thick disk has a large vertical scale length of 1-1.5 kpc with vertical velocity dispersion of 45 km s^{-1} .

In many research, it is found that the distribution of chemical abundance and age of the thick disk stars are not uniform, they are varying with galactocentric distance. Stars having metal-poor chemical abundances generally found in the thick are at a solar radial distance and the metal-rich stars are found outside of that radial distance. Additionally, the recent observations have reported that the average stellar age of thick disk stars quickly decreases as one moves from the inner to the outer disk [5].

1.1.3 The Bulge

The galactic bulge is a tightly packed group of stars within a larger formation of stars. Initially, the bulge was believed to be an elliptical galaxy with a disk of stars around them but later Hubble Space Telescope revealed bulge lie at the heart of a spiral galaxy.

The bulge has a scale height of 0.4 kpc and velocity distribution of about 100 km s^{-1} . The bulge is about 1/3 of the mass of the disk and there is considerable evidence that shows the bulge contains a bar. The bulge is considered mysterious as most of the information obtained is based on the property of the star in Baade's window. IRS, COBE, and ISO have provided information about the structural properties of

the bulge. There is not an accurate prediction of the age of bulge stars and also the age of bulge itself. Several studies agree upon bulge to be 5 – 8 Gyr old but there is evidence that suggests it to be approximately 15 Gyr old [2].

1.1.4 The Galactic Halo

As mentioned above galactic halo has two components. The dark halo extends to over 200 kpc and has a total mass of $10^{12} M_{\odot}$ (solar mass). The dark halo existence can be derived for example, from motions of satellites of the Milky Way or from timing arguments of binary system M31-Milky Way.

The stellar halo is less important dynamically but it contains metal-poor stars and old ones, it can provide the picture of the early stage of the galaxy. The stellar halo has a total luminosity in range $8 \times 10^8 L_{\odot} - 10^9 L_{\odot}$. Its luminosity profile fits $r^{-3.5}$ law. The stellar halo shows no systematic rotation with $V_{\phi} = 3 \pm 21 \text{ km s}^{-1}$, $V_r = 16 \pm 18 \text{ km s}^{-1}$ and $V_z = 10 \pm 12 \text{ km s}^{-1}$ but there is evidence that suggests retrograde motion in outer region.

Halo stars are among oldest star in the galaxy but still there have been a detection of few metal-rich A stars along with some A and F main-sequence stars with halo kinematics. These stars are of intermediate age and might have originated from a satellite galaxy that was accreted in the past 10 Gyr [2].

1.2 Motivation

My project work is focused on the kinematics of stars located in the halo of the Milky Way galaxy. I will be taking the data collected by

Gaia and GALAH observation for my research. For this project work, I was inspired by many researcher's work and their papers. Some works in this field allured me to drive my knowledge to study how metal-poor stars are dynamically distributed in the inner halo and out halo regions of our home Galaxy; and what are the relation between metallicity with phase space velocities of these stars. There are the following grounds to motive this research project that is organized below.

- Hao Tian and his team(2019) [6] studied K-giants within 4 kpc using the Gaia and LAMOST data. In their research, they found the prograde motion of inner halo with speed 27_{-5}^{+4} km s $^{-1}$. They also reported that the rotational velocity is independent of metallicity within the local volume which is considerably different from other previous research. Besides this, they also noticed out component of the metal-poor thick disk and counter-rotating hot component.
- Prajwal R. Kafle and his team(2017) [7] studied the rotation-metallicity bias in the inner stellar halo of the Milky Way. In their paper, they discussed the importance of the first-order moment and second-order moment as they possess information about the early development of the Galaxy. They found out that MSTO, BHB metal-rich stars are in prograde motion and metal-poor stars are in retrograde motion but lagging observed for K-giant are very small. They also discussed about the metallicity dependence of velocity moments.
- Sarah A. Bird (2019) [8] studied the anisotropy of the stellar halo using K-giant from Gaia and LAMOST, where they have mentioned the importance of β to determine whether orbit is predominantly radial or tangential. In their study, they showed V_r , V_θ , V_ϕ as a

function of metallicity and galactocentric distance. They found out from solar position to 25 kpc orbit are highly radial then decline to isothermality.

1.3 Objective

Following are the major objectives of my research work:

- To determine the rotational velocities of the Milky Way stellar halo.
- To study the relationship between the rotational velocity and metallicity.
- To determine the velocity anisotropy and its relationship with metallicity.
- To establish the relation between angular momentum and energy of these stars.

1.4 Significance of the Study

Following are the significance of my research work:

- Study of the rotational velocity can tell us about the retrograde and prograde motion of star.
- Study of the variation of rotational velocity with metallicity can tell us about the effect of metallicity on the kinematics of star.
- Study of anisotropy parameter β tell us about the extent to which stellar system is predominantly radial or tangential.

- First order and second order moment is very useful to study formation of galactic halo as they posses the information regarding formation.
- This study can give better picture regarding effect of metallicity to motion and distribution of star.
- This study give us idea regarding distribution of β anisotropy with galactocentric radius and effect of metallicity on it.
- The comparison of kinematics of old star (i.e metal poor) with younger star (i.e metal rich) give us knowledge about the evolution of star with the time.

1.5 Limitations of the Study

Following are the significance's of my research work:

- Our Research focuses on only K-giant stars but other types of stars also provide a signature of galaxy formation.
- Due to large parallax uncertainty in the Gaia data-set at a far distance, we had to reduce far distant stars using $\text{parallax_over_error} > 5$, thus we could not able to study the stars beyond 20 kpc from the Galactic center.

Chapter 2

Theory

2.1 Parallax

Parallax is derived from Ancient Greek 'parallaxis' which means alternation. Parallax is displacement or difference in apparent position of object viewed along two line of sight and it is measured by angle or semi-angle of inclination along these two line. Astronomer has used principle of parallax to determine distance between celestial bodies.

To be more specific about parallax for astronomy we must discuss about stellar parallax. Stellar parallax is apparent shift in position of the star against the distant object in the background. Stellar parallax is often measured using annual parallax which can be simply explained as difference between position of star viewed from sun and earth or can be understood as angle made by mean radius of orbit with the star nearby.

From Fig. 2.1, we can write;

$$\tan p = \frac{1\text{AU}}{d} \quad (2.1)$$

where p is parallax and d is distance of star, further for small p we can write :

$$\tan p \approx p$$

$$d = \frac{1}{p} \quad (2.2)$$

We get distance of star in parsec when parallax is in arcseconds. This method is popularly used in determining the distance of distant celestial body.

To explain the working mechanism of parallax, we consider a pencil shifting method as parallax. In this method, we extend our arm and observe the position of pencil by the right eye while the left eye is closed. By doing so, we can observe the shift in its position.

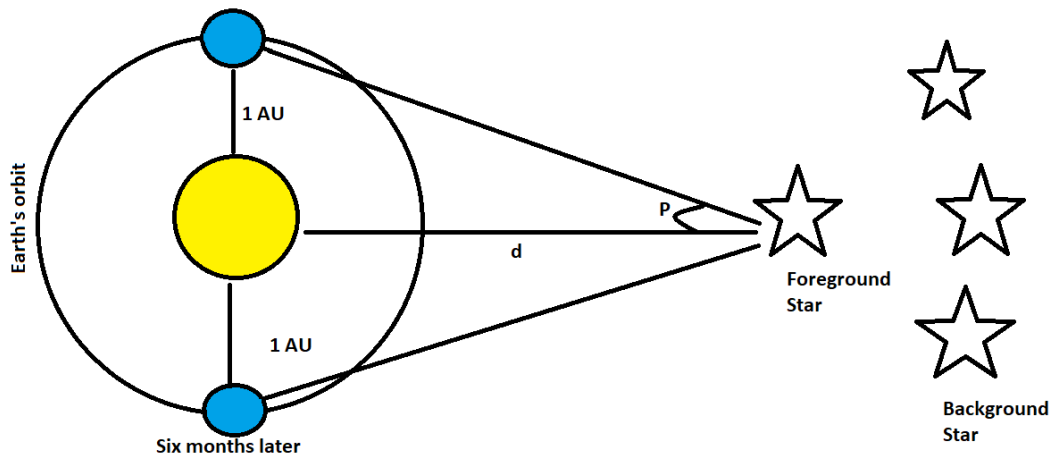


Figure 2.1: Stellar parallax of star with parallax (p) situated at distance (d) from the Sun, where 1 AU (Astronomical Unit) is distance between the Sun and Earth.

2.2 Proper Motion

Stars appear to maintain a fixed position relative its neighbor stars, so we see fix the shape of the constellation. But in reality over a long

period of time, this constellation changes its shape which means stars are in independent motion. This motion is caused by the movement of the star relative to the Sun and solar system.

So, we can define the proper motion as astrometric measure of the observed changes in the position of the stars and celestial bodies as observed from the Sun. It is generally measured in arcseconds (as/yr) per year or milliarcsecond per year (mas/yr) [8]. It is a 2-dimensional vector that can be defined by two quantities - position angle and its magnitude. The first quantity gives the direction of motion in the celestial sphere and the second quantity gives motion's magnitude.

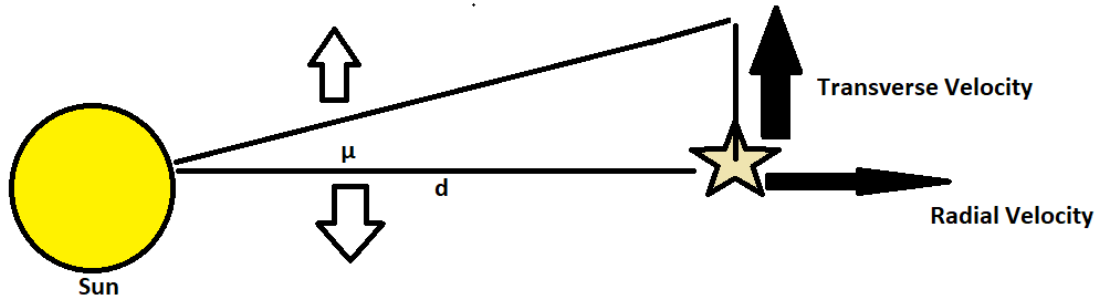


Figure 2.2: Proper motion of the star.

2.3 Velocity Anisotropy

Velocity anisotropy characterizes the extent to which orbits in the stellar system are predominantly tangential, isotropic, or radial. It is denoted by the symbol β . If $\sigma_r(r)$ be velocity dispersion along the radial vector and $\sigma_t(r)$ be velocity dispersion along perpendicular direction then velocity anisotropy is given as: [10]

$$\beta = 1 - \frac{\sigma_t^2}{\sigma_r^2} \quad (2.3)$$

In spherical coordinate system with dispersion of velocities ($\sigma_r, \sigma_\theta, \sigma_\phi$), the beta anisotropy can be defined as:

$$\beta = 1 - \frac{\sigma_\theta^2 + \sigma_\phi^2}{2\sigma_r^2} \quad (2.4)$$

The value of β lie in between $(-\infty, 1)$ and as mentioned above it gives us idea about overall structure of halo in following manner:

- If $\beta < 0$ then it means orbit is tangentially biased.
- If $\beta = 0$ then it means orbit is isotropic.
- If $\beta > 0$ then it means orbit is radially biased.

Here, we can see β is a highly asymmetric function around the isotropic. So, it is quite sensible to use a modified version of anisotropy, $\frac{\beta}{2-\beta}$ whose value lies in between $[-1, 1]$. And other conditions remain similar to those mentioned above.

Further, we can express the Jeans equation in terms of velocity anisotropy. Assuming the mass to be 1 in spherical coordinate we can write momentum as : [11]

$$p_r = \dot{r} = v_r \quad (2.5)$$

$$p_\phi = r^2 \sin \theta \dot{\phi} = r^2 \sin \theta v_\phi \quad (2.6)$$

$$p_\theta = r^2 \dot{\theta} = r^2 v_\theta \quad (2.7)$$

Now, we can write the Hamiltonian as:

$$H = \frac{1}{2} \left(p_r^2 + \frac{p_\theta^2}{r^2} + \frac{p_\phi^2}{r^2 \sin^2 \theta} \right) + \phi(r) \quad (2.8)$$

Further, we have from collisionless Boltzmann equation as :

$$\frac{\partial f(q, p, t)}{\partial t} + \dot{q} \frac{\partial f(q, p, t)}{\partial q} + \dot{p} \frac{\partial f(q, p, t)}{\partial p} = 0 \quad (2.9)$$

Using $\dot{q} = \frac{\partial H}{\partial p}$ and $\dot{p} = -\frac{\partial H}{\partial q}$

Now, equation (2.9) can be written as :

$$p_r \frac{\partial f}{\partial r} + \frac{p_\theta}{r^2} \frac{\partial f}{\partial \phi} + \frac{p_\phi}{r^2 \sin^2 \theta} \frac{\partial f}{\partial \phi} - \left(\frac{d\phi}{dr} - \frac{p_\theta^2}{r^3} - \frac{p_\theta^2}{r^3 \sin \theta} \right) \frac{\partial f}{\partial p_r} + \frac{p_\phi^2 \cos \theta}{r^2 \sin^3 \theta} \frac{\partial f}{\partial p_\theta} = 0 \quad (2.10)$$

We multiply by p_r above then integrate over all (p_r, p_θ, p_ϕ) using $dp_r dp_\theta dp_\phi = r^2 \sin \theta dv_r dv_\theta dv_\phi$ then we do partial integration so it can be written as:

$$\frac{\partial(r^2 \sin \theta \bar{v}_r^2)}{\partial r} + \frac{\partial(\sin \theta \nu \bar{v}_r \bar{v}_\theta)}{\partial \theta} + \frac{\partial(\frac{\nu \bar{v}_r \bar{v}_\theta}{\sin \theta})}{\partial \phi} + r^2 \sin \theta \nu \left(\frac{d\phi}{dr} - \frac{\bar{v}_\theta^2}{r} - \frac{\bar{v}_\phi^2}{r} \right) = 0 \quad (2.11)$$

Since all odd order moment of v_r are vanished above equation can be written as :

$$\frac{d(\nu v_r^2 r)}{dr} + \nu \left(\frac{d\phi}{dr} + \frac{2\bar{v}_r^2 - v_\phi^2 - v_\theta^2}{r} \right) = 0 \quad (2.12)$$

We know:

$$\beta = 1 - \frac{\sigma_\theta^2 + \sigma_\phi^2}{2\sigma_r^2} \quad (2.13)$$

$$\beta = 1 - \frac{\bar{v}_\theta^2 + \bar{v}_\phi^2}{2\bar{v}_r^2} \quad (2.14)$$

Finally substituting this on 2.12 we get:

$$\frac{d(\nu v_r^2)}{dr} + 2\frac{\beta}{r} \nu v_r^2 = -\nu \frac{d\phi}{dr} \quad (2.15)$$

This is required for the spherical Jeans equation in terms of the anisotropy parameter for a non-rotating system.

2.4 Metallicity

Most of the universe is filled with hydrogen and helium. Astronomers use the term metal to represent all other elements except hydrogen and helium. So, metallicity is an abundance of elements other than hydrogen and helium present in an object. So, when the star is said to be metal-rich it means the star has a dense amount of elements other than hydrogen and helium.

Based on metallicity Walter Baade divided stars into two populations namely Population I (metal-rich) and Population II (metal-poor) stars. Later on, Population III stars were added which are the metal poorest star and they are believed to be the firstborn star.

Metallicity is expressed in term of abundance ratio and it is defined as the logarithm of the ratio of a star's iron abundance compared to that of the Sun and is expressed thus: [12]

$$[Fe/H] = \log_{10}\left(\frac{N_{Fe}}{N_H}\right)_{star} - \log_{10}\left(\frac{N_{Fe}}{N_H}\right)_{sun} \quad (2.16)$$

where N_{Fe} and N_H is no. of iron and hydrogen atom per unit volume. Unit used to measure metallicity is decimal exponent (dex). Here star with metallicity greater than sun has positive logarithmic value, those with lower metallicity than sun has negative logarithmic value and it is zero for star with metallicity equal to that of sun.

Population I has significantly high value of $[Fe/H]$ compare to

Population II and Population III. Population III star are very poor that there metallicity is lower than -6 .

2.5 K-giant

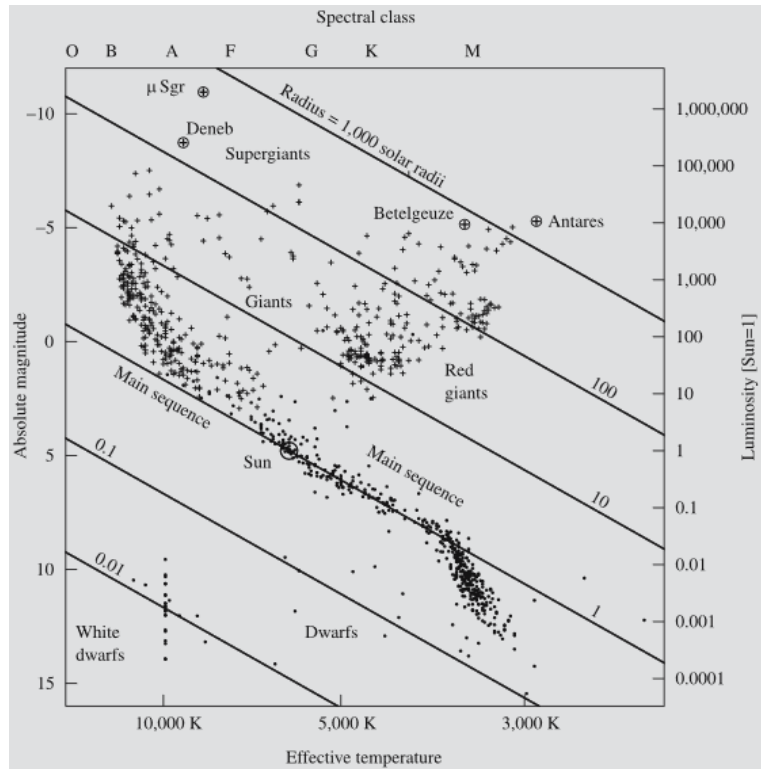


Figure 2.3: H-R diagram, here we can see the position of stars divided according to temperature, spectral class, luminosity and absolute magnitude. [1]

K-giants are luminous and are of large radius compared to main-sequence stars, which enable us to study the dynamic of the galaxy even beyond the solar neighborhood. In the HR diagram, the giants are placed just above the main sequence stars. Further, these giants stars can be classified into several groups, the horizontal branch is an almost horizontal sequence with an absolute magnitude of almost 0 [1]. The red giant branch rises almost vertically from the main sequence at spectral types K and M in the HR diagram [1]. Finally, the asymptotic

branch rises from the horizontal branch and approaches the bright end of the red giant branch. It should be remembered that this giant phase represent the different phase of stellar evolution [1].

2.6 Gaussian Distribution

According to Central Limit Theorem all other distribution converges to Gaussian distribution as sample size increases $n \rightarrow \infty$. It is so because Gaussian distribution act as an attractor in fundamental functional space of probability density function [13]. A random variable ' x ' is said to be the Gaussian distribution if its probability density function is defined as:

$$f(x) = \frac{1}{\sqrt{2\pi}\sigma^2} e^{-\frac{1}{2}\frac{(x-\mu)^2}{\sigma^2}}, -\infty < x < \infty, -\infty < \mu < \infty, \sigma > 0 \quad (2.17)$$

Where μ is a mean of x and σ^2 is variance of the x . Gaussian distribution is also commonly referred as normal distribution. For the Gaussian distribution mean, median and mode are same. Further we have characteristics function $\phi(t)$ of normal distribution as:

$$\phi(t) = \exp(it\mu - \frac{1}{2}\sigma^2t^2) \quad (2.18)$$

We can define a standard normal variate as:

$$z = \frac{x - \mu}{\sigma} \quad (2.19)$$

Using this variate we can have a probability density function given as:

$$f(z) = \frac{1}{\sqrt{2\pi}} e^{-\frac{1}{2}z^2}, -\infty < z < \infty \quad (2.20)$$

In case of variate z has a mean $\mu=0$ and variance $\sigma^2=1$. So, now, we have characteristics function of z as:

$$\phi(t) = \exp\left(-\frac{1}{2}\sigma^2 t^2\right) \quad (2.21)$$

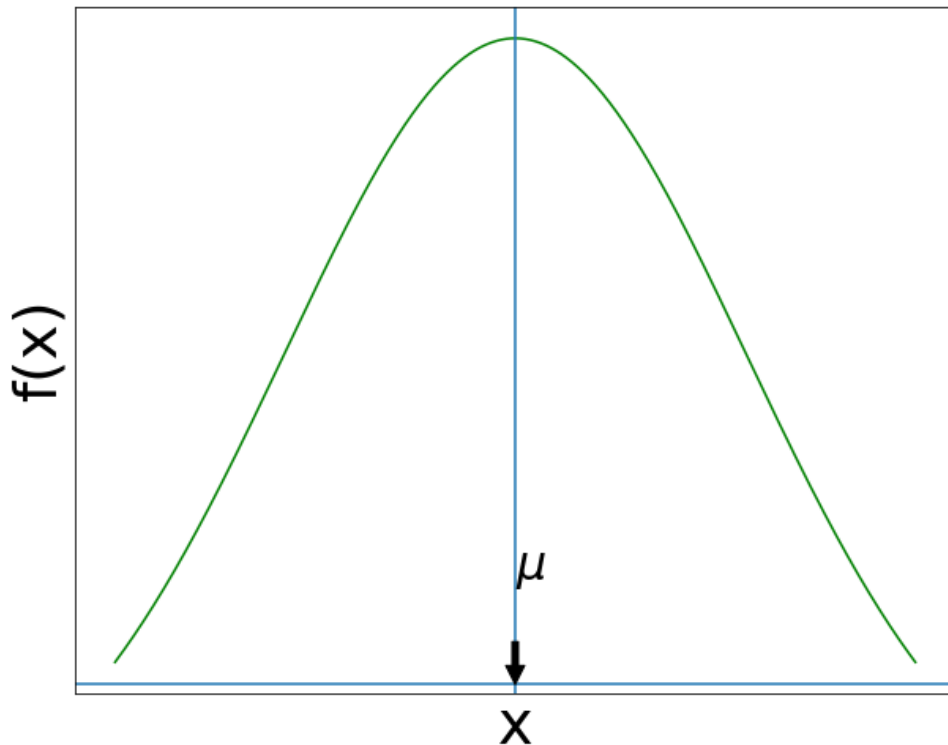


Figure 2.4: Probability density function of the Gaussian distribution with mean μ and variance σ^2 .

2.7 Bayes' Theorem

Bayes' theorem was given by the Thomas Bayes in 1763, it is foundation of Bayesian inference. Bayes' theorem is used to determine the conditional probability distribution. Suppose A and B are two events

then conditional probability of A given B can be written as:

$$p(A|B) = \frac{p(A \cap B)}{p(B)} \quad (2.22)$$

Similarly we can write for $p(B|A)$ as:

$$p(B|A) = \frac{p(B \cap A)}{p(A)} \quad (2.23)$$

$$p(B \cap A) = p(A) p(B|A) \quad (2.24)$$

Now we can write $p(A|B)$ as:

$$p(A|B) = \frac{p(A) p(B|A)}{p(B)} \quad (2.25)$$

This equation (2.32) is required expression for Bayes' theorem. Here $p(A|B)$ is a conditional probability of likelihood of A given B is true, similarly $p(B|A)$ is a conditional probability of likelihood of B given A is true and $p(A)$, $p(B)$ are probability of A and B which are often referred as marginal probability of A and B respectively. It has most important theory as it form foundation of entire Bayesian statistics.

2.8 Markov Chain Monte Carlo (MCMC)

MCMC methods are methods for sampling the probability density function. For MCMC we don't need an analytical description of fully normalized pdf for sampling so, it is ideal for sampling the posterior distribution [14]. If we have data D with parameter θ then we can write posterior pdf as:

$$p(\theta|D) = \frac{1}{p(D)} p(D|\theta)p(\theta) \quad (2.26)$$

$$p(\theta/D) = \frac{1}{Z} p(D|\theta) p(\theta) \quad (2.27)$$

This is a Bayes' theorem. In above equation $p(D|\theta)$ is a likelihood function and $p(\theta)$ is prior pdf. Further Z or $p(D)$ is called marginal pdf or evidence and it is often difficult to determine. For MCMC sampling we don't need evidence Z . Further we have:

$$p(\theta/D) \propto p(D|\theta)p(\theta) \quad (2.28)$$

Implementation of MCMC can be described on following steps:

1. Initially, we need to define a modeling function based on the model parameters.
2. We define an ensemble of walkers defined by a θ vector that contains a set of parameters used by the model generating function.
3. Each walker starts to explore the parameter space. These walkers take a new value of θ and generate the model that corresponds to θ then compare the model correspond to data.
4. Now decision to move on a new position is based on the ratio of likeliness generated by a new model to likeliness generated by an old model i.e. if a new location is better matched to data then walker move to a new location otherwise it stays on the previous location.

But this is not always a case, sometimes in a new location it is taken into consideration even though it is not good as the previous one or a new location is not taken into consideration even though it is worse than the previous one. This is governed by the

acceptance ratio. The advantage of this approach is that all walker doesn't get trapped in the individual peak of probability

5. Repeating this step by walkers begin to climb toward region of highest likelihood.

After completion of above step we get the posterior distribution. Often, MCMC is confused or used as an optimizer but it should be kept in mind that MCMC is a sampler, it samples over the parameter space what we have defined. So, what MCMC is best at is in sampling the ill normalized distribution.

2.9 Energy and Angular Momentum

The total energy of the star is given by the sum of the kinetic energy and potential energy of the star. The kinetic energy of the star can be expressed as: [8]

$$\text{Kinetic Energy} = \frac{V_{tot}^2}{2} \quad (2.29)$$

Where $V_{tot}^2 = V_r^2 + V_\theta^2 + V_\phi^2$ is a total velocity of star. Although the measurement of kinetic energy is quite straightforward for stars, the measurement of potential energy is not that straightforward. In our research work, we used McMillian potential (Mc Millan *et al.* (2017)) as it sums up all the Milky Way potential components. He put forward six axisymmetric components of the Milky Way which are briefly described below; [15]

- **The Bulge:**

The density profile of bulge can be defined as, in cylindrical coordinate system;

$$\rho_b = \frac{\rho_{o,b}}{(1 + r^1/r_o)^\alpha} \exp[-(r^1/r_{cut})^2] \quad (2.30)$$

Here, $r^1 = \sqrt{R^2 + (z)^2}$, $r_o = 0.075$ kpc, $r_{cut} = 2.1$ kpc, axis ratio $q = 0.5$, $M_b = 8.9 \times 10^9 M_o \pm 10\%$ and $\rho_{o,b} = 9.93 \times 10^{10} M_o$ kpc $^{-3} \pm 10\%$.

- **The Stellar Discs:** This is one of the axisymmetric components of the Milky Way whose density profile can be expressed as

$$\rho_d(R, z) = \frac{\Sigma_o}{2z_d} \exp\left(-\frac{|z|}{z_d} - \frac{R}{R_d}\right) \quad (2.31)$$

Here, z_d = scale height, R_d = scale length, Σ_o = central surface density, $M_d = 2\pi\Sigma_o R_d^2$.

- **The Gas Discs:**

The density profile of the gas disk can be expressed as;

$$\rho_d(R, z) = \frac{\Sigma_o}{4z_d} \exp\left(-\frac{R_m}{R} - \frac{R}{R_d}\right) \operatorname{sech}^2(z/2z_d) \quad (2.32)$$

Here, the disc has a hole at centre with associated scale length R_m and other notation is similar to stellar discs above.

- **The Dark Matter Halo:**

The density profile of the dark-matter halo can be expressed as

$$\rho_h = \frac{\rho_{0,h}}{x^2(1+x)^2} \quad (2.33)$$

Here, $x=r/r_h$ where r_h is scale radius. If we choose γ , we can get the

value of density profile of eq. (2.33) from the following equation.

$$\rho_h = \frac{\rho_{0,h}}{x^\gamma(1+x)^\gamma}$$

This gives the **NFW** density profile of dark-matter halo (Navarro, Frenk, & White (1996)).

Once we get the kinetic energy and potential energy (Φ) by method as mentioned above we can write total energy as:

$$E = \frac{V_{tot}^2}{2} + \Phi \quad (2.34)$$

Further, for the evaluation of angular momentum of K-giant, we use following relation (S. Bird *et al.* (2018), reference therein): [8]

$$L = r_{gc} V_{tan} \quad (2.35)$$

Here, r_{gc} is galactocentric radius and V_{tan} is tangential velocity (i.e. $V_{tan}^2 = V_\theta^2 + V_\phi^2$).

2.10 Gaia

European Space Agency (E.S.A) launched the Gaia mission in 2013 which is a successor of their previous Hipparcos mission. Gaia is by far the biggest stellar census ever launched it has created a 3-dimensional space catalog of more than a billion stars. Besides stars, it also collects the data of planets, asteroids, and quasars. So, Gaia has a huge data set that consists of precise 3-dimensional information of stars.

If we look at the Gaia satellite then its instrument can be classified into mainly three parts:

Astrometry Instrument :

Astrometry instrument accurately determine the position of a star with

a magnitude greater than 20 by measurement of their angular position [16].

Photometric Instrument :

The photometric instrument (BP/RP) allows the acquisition of luminosity measurements of stars over the 320–1000 nm spectral band, of all stars brighter than magnitude 20.7 [15].

Radial – Velocity Spectrometer :

Velocity of the celestial objects along the line of sight is determined using the Radial-Velocity Spectrometer (RVS). RVS does this measurement by acquiring high-resolution spectra in spectral band 847 - 874 nm (field lines of calcium ion) for objects up to magnitude 17. Radial velocities are measured with a precision between 1 km s^{-1} ($V=11.5$) and 30 km s^{-1} ($V=17.5$) [17].

2.11 GALACTIC Archaeology with HERMES (GALAH)

The GALactic Archaeology with HERMES (GALAH) survey is a Large Observing Program using the HERMES instrument with the Anglo-Australian Telescope of the Australian Astronomical Observatory [18]. HERMES is capable of providing spectra of 400 bodies on 4 different spectra simultaneously. This information is important to determine the chemical abundance of particular body. GALAH will obtain the radial velocities and elemental abundance of approximately one million stars [18]. This information will provide us information about the evolution of universe with a time, importance of merger, history of formation of star and change in stellar dynamics over a time [18].

Chapter 3

Data & Method

3.1 Data

Recently Gaia published their Gaia EDR3 which consists of the celestial positions and apparent brightness of about 1.8 billion sources [19]. Among 1.8 billion sources parallaxes, proper motions, and the colour (G_{BP} - G_{RP}) of 1.5 billion sources are available [19]. Among all these, 7 million stars are accompanied by their radial velocity [19]. Gaia has increased precision in the measurement of parallax and proper motion in EDR 3 compare to DR2 but radial velocities are the same as in DR2 [19].

GALAH has released there DR3 which consist of 5,88,571 stars information among which 3,83,088 (65%) dwarfs, 2,00,927 (34%) giants and 4,556 (1%) other/unclassified stars [20]. Based on unflagged chemical composition and age, they found 62.5% young low - α stars, 8.8% young high- α stars, 26.9% old stars, and 1.8% stars with metallicity less than -1 [20]. Among all of these, there are about 4% halo stars [20].

Although Gaia consist of all the astrometric information needed for us but it doesn't contain the some of information which we needed like temperature, logg, metallicity ([Fe/H]). So, to get this information, we

cross match the GALAH data with Gaia. Among all the data we selected the K-giant stars using the following criteria as given in Liu *et al.* (2014) ; [21]

1. $4000 < T_{eff}/k < 4600$, $\log g < 3.5$ dex
2. $4600 < T_{eff}/k < 5600$, $\log g < 4$ dex

Initially, we got 5,86,753 stars but after using the above selection criteria, we were left with 41,486 K-giant stars. Further, we filtered the data to take stars with metallicity -0.5 to -2.5 and within the solar neighbourhood (i.e $4\text{kpc} < R < 12\text{kpc}$). Among these further, we selected only those K-giant stars with velocities as $-600 < V_R < 600$, $-600 < V_T < 600$ and $-600 < V_Z < 600$. With this we have only 3081 K-giant stars left and further work is based on these data. All data collection and cross-matching are done using an in-built function of gaia_tools (https://github.com/jobovy/gaia_tools). In our analysis. we have taken $R_\odot = 8.21$ kpc [15], $z = 25.0$ pc [22], $(U_\odot, V_\odot, W_\odot) = (11.1 \text{ km s}^{-1}, 15.17 \text{ km s}^{-1}, 7.25 \text{ km s}^{-1})$ and $V_{LSR} = 232 \text{ km s}^{-1}$ [23]. The logg versus Temperature plot of the entire dataset and selected star is given below:

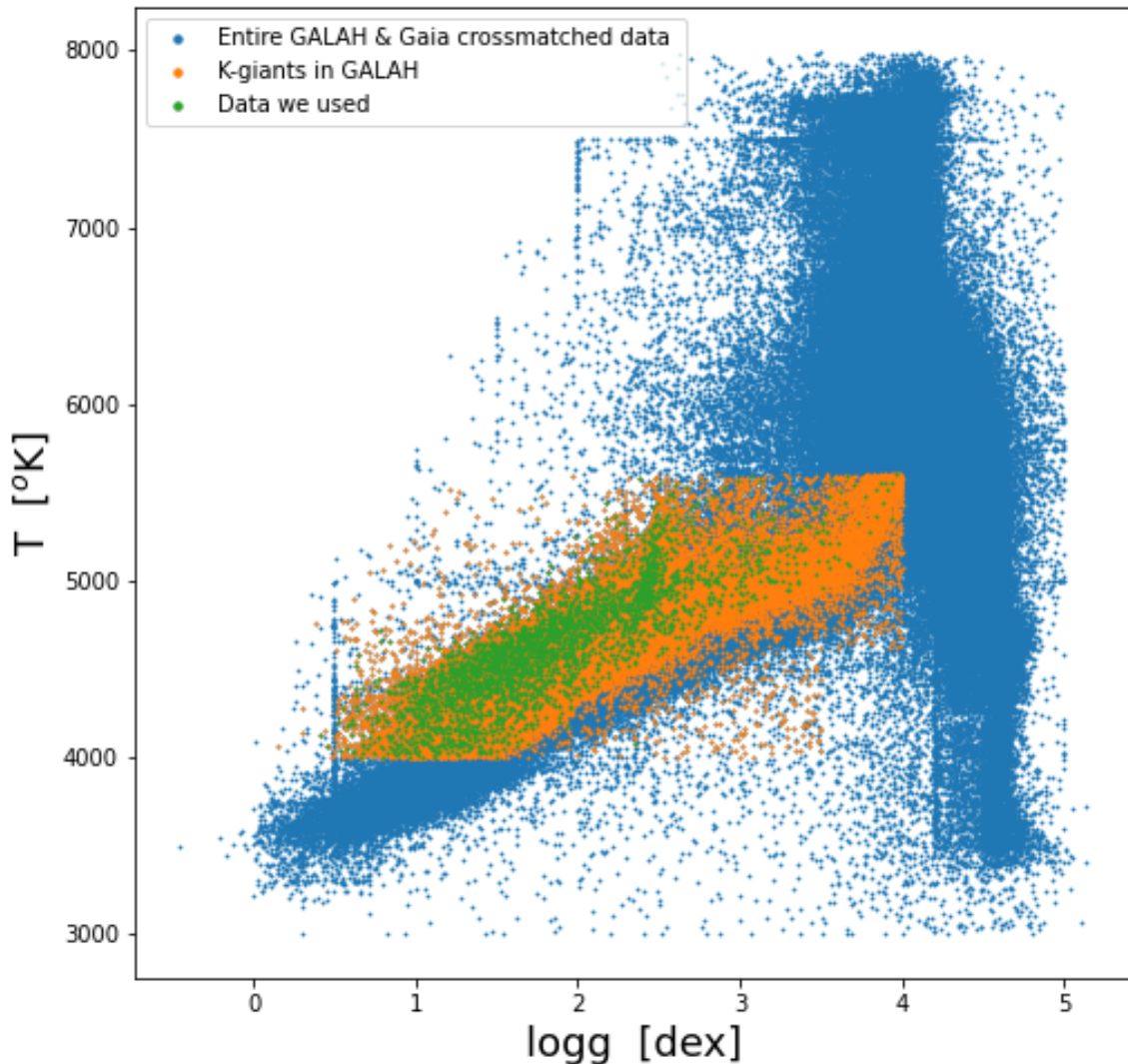


Figure 3.1: Temperature versus $\log g$ plot for entire dataset of GALAH cross-matched with Gaia (represented by blue dot), K-giant stars in GALAH (represented by orange dot) and K-giant stars selected for our research (represented by green dot).

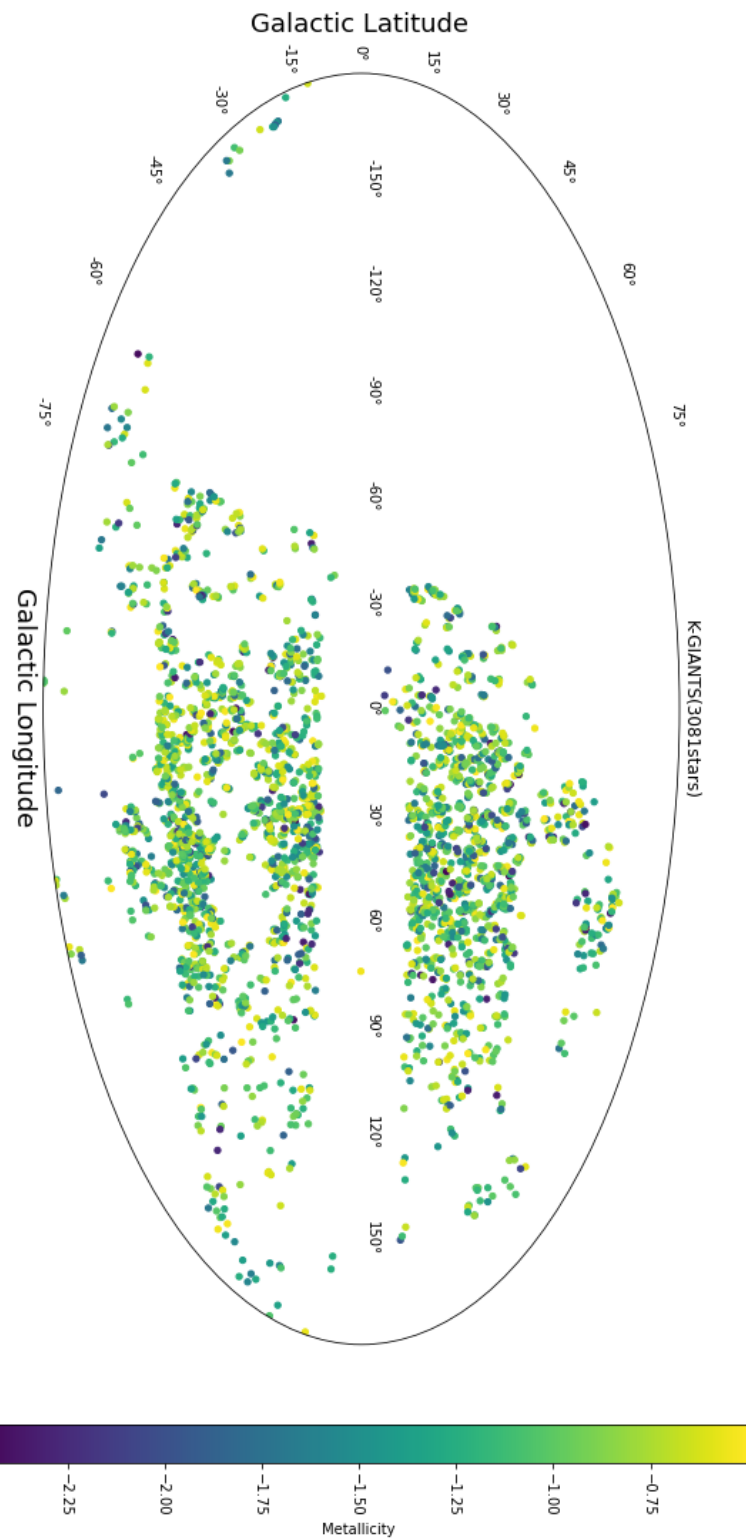


Figure 3.2: Mollweide projection of selected K-giant stars with the color bar representing there metallicity [Fe/H]

3.2 Method

3.2.1 Transformation of Coordinates and Velocity

Johnson *et al.* [24] mentioned that there are three angles that defines the galactic coordinate system. Out of three 2 gives the position of the North Galactic Pole (NGP) i.e. $\alpha_{NGP} = 192.5^\circ$, $\delta_{NGP} = 27.4^\circ$ [24]. Third angle $\theta_o = 123^\circ$ gives the position of North Celestial Pole relative to great semicircle passing through the NGP and zero galactic latitude [24]. Galactic coordinate can be calculated from the equatorial coordinate using following relation (D. R. H. Johnson and D. R. Soderblom (1987)): [24]

$$\begin{bmatrix} \cos b \cos l \\ \cos b \sin l \\ \sin b \end{bmatrix} = \mathbf{T} \begin{bmatrix} \cos \delta \cos \alpha \\ \cos \delta \sin \alpha \\ \sin \delta \end{bmatrix} \quad (3.1)$$

Where l is galactic longitude, b is galactic latitude, α is right ascension, δ is declination, all of them are in degree. Here, transformation matrix \mathbf{T} is given as:

$$\mathbf{T} = \begin{bmatrix} +\cos \theta_o & +\sin \theta_o & 0 \\ +\sin \theta_o & -\cos \theta_o & 0 \\ 0 & 0 & +1 \end{bmatrix} \begin{bmatrix} -\sin \delta_{NGP} & 0 & +\cos \delta_{NGP} \\ 0 & -1 & 0 \\ +\cos \delta_{NGP} & 0 & +\sin \delta_{NGP} \end{bmatrix} \begin{bmatrix} +\cos \alpha_{NGP} & +\sin \alpha_{NGP} & 0 \\ +\sin \alpha_{NGP} & -\sin \alpha_{NGP} & 0 \\ 0 & 0 & 1 \end{bmatrix} \quad (3.2)$$

On substituting the value of α_{NGP} , δ_{NGP} and θ_o we get

$$\mathbf{T} = \begin{bmatrix} -0.06699 & -0.87276 & -0.48354 \\ +0.49273 & -0.45035 & +0.74458 \\ -0.86760 & -0.18837 & +0.46020 \end{bmatrix} \quad (3.3)$$

We further define the coordinate matrix:

$$\mathbf{A} = \begin{bmatrix} +\cos\alpha\cos\delta & -\sin\alpha & -\cos\alpha\sin\delta \\ +\sin\alpha\cos\delta & +\cos\alpha & -\sin\alpha\sin\delta \\ +\sin\delta & 0 & +\cos\alpha \end{bmatrix} \quad (3.4)$$

The galactic space velocity components are:

$$\begin{bmatrix} \mathbf{U} \\ \mathbf{V} \\ \mathbf{W} \end{bmatrix} = \mathbf{T} \cdot \mathbf{A} \begin{bmatrix} \rho \\ \frac{k\mu_\alpha}{\pi} \\ \frac{k\mu_\beta}{\pi} \end{bmatrix} = \mathbf{B} \begin{bmatrix} \rho \\ \frac{k\mu_\alpha}{\pi} \\ \frac{k\mu_\delta}{\pi} \end{bmatrix} \quad (3.5)$$

Where $\mathbf{B} = \mathbf{T} \cdot \mathbf{A}$ and $k = 4.74057$, μ_α is proper motion along right ascension, μ_δ is proper motion along the declination.

We can obtain the 6 dimensional information given by Gaia in term of Cartesian coordinate using following relation (It should be noted that following position and velocity is barycentric): [25]

In the galactic coordinate system the components of the normal triad $[\hat{p} \hat{q} \hat{r}]$ are given by:

$$R = \begin{bmatrix} p_x & q_x & r_x \\ p_y & q_y & r_y \\ p_z & q_z & r_z \end{bmatrix} = \begin{bmatrix} -\sin l & -\sin b \cos l & \cos b \cos l \\ \cos l & -\sin b \sin l & \cos b \sin l \\ 0 & \cos b & \sin b \end{bmatrix} \quad (3.6)$$

Here, \hat{r} is a unit vector that specifies barycentric coordinate direction, \hat{p} and \hat{q} are unit vectors in directions of l and b ar \hat{r} . So now barycentric

positions and velocities can be given as : [25]

$$\begin{bmatrix} r_x^b \\ r_y^b \\ r_z^b \end{bmatrix} = R \begin{bmatrix} 0 \\ 0 \\ \frac{A_p}{\bar{w}} \end{bmatrix} \quad (3.7)$$

$$\begin{bmatrix} V_x^b \\ V_y^b \\ V_z^b \end{bmatrix} = R \begin{bmatrix} \frac{\mu_{l*} A_v}{\bar{w}} \\ \frac{\mu_b A_v}{\bar{w}} \\ v_{rad} \end{bmatrix} \quad (3.8)$$

Here $A_p = 1000$ mas pc and $A_v = 4.74047\text{yr km/s}$ designate the astronomical unit in the appropriate form.. This is required equation needed to evaluate position and velocity using the Gaia parameters l (galactic longitude), b (galactic latitude), \bar{w} (parallax) , μ_{l*} (proper motion along the l), μ_b (proper motion along the b) and v_{rad} (radial velocity).

It should be noted that all of this work is done using the inbuilt function on galpy package [26].

3.2.2 Relationship between the Cartesian Coordinate, Spherical Coordinate and Cylindrical Coordinate

We use equations (3.6) and (3.7) to evaluate positions and velocities in the Cartesian coordinate. After that, we use the transformation equations for spherical to transfer the Cartesian positions and velocities using the Orbit function of galpy. The relationship between Cartesian and spherical coordinate system is given below; [8]

$$r = \sqrt{x^2 + y^2 + z^2} \quad (3.9)$$

$$\theta = \frac{\pi}{2} - \tan^{-1}\left(\frac{z}{\sqrt{x^2 + y^2}}\right) \quad (3.10)$$

$$\phi = \tan^{-1}\left(\frac{y}{x}\right) \quad (3.11)$$

In this way we convert position in Cartesian coordinate (x, y, z) to spherical coordinate (r, θ, ϕ). Further for conversion of velocity from Cartesian (V_x, V_y, V_z) to spherical (V_r, V_θ, V_ϕ) we have following relation: [8]

$$V_r = (V_x \cos \phi + V_y \sin \phi) \sin \theta + V_z \cos \theta \quad (3.12)$$

$$V_\theta = (V_x \cos \phi + V_y \sin \phi) \cos \theta - V_z \sin \theta \quad (3.13)$$

$$V_\phi = -V_x \sin \phi + V_y \cos \phi \quad (3.14)$$

Now, to convert Cartesian coordinate system to cylindrical coordinate, we have used the inbuilt function of galpy [26] which uses the following relations:

$$R = \sqrt{x^2 + y^2} \quad (3.15)$$

$$\phi = \tan^{-1}\left(\frac{y}{x}\right) \quad (3.16)$$

$$Z = z \quad (3.17)$$

Further, galpy [24] uses following relation to determine the cylindrical velocity from Cartesian:

$$V_R = V_x \cos \phi + V_y \sin \phi \quad (3.18)$$

$$V_T = -V_x \sin \phi + V_y \cos \phi \quad (\because V_T = V_\phi) \quad (3.19)$$

$$V_Z = V_z \quad (3.20)$$

These are relation which we use to convert one coordinate system to other.

3.2.3 Determination of Rotational Velocity

If we move along the galactic plane then we find a mixture of the MWTD and inner halo within the 5 kpc of the plane, above it, till 10 kpc there is a dominance of the inner halo and beyond the 20 kpc, the outer halo dominates [27]. But in between 15-20 kpc there is an inversion point of the dominance of the inner halo and outer halo [27]. In our sample, we have data ranging from $-17.64 \text{ kpc} < Z < 15.8 \text{ kpc}$. So, we believe that there should be three components in our sample. Further, we assumed these three components to be Gaussian as suggested in Tian *et al.* [6].

So the distribution of these components can be written as:

$$p_i(V_T^{(k)}|f_i, V_{T,i}, \sigma_i) = \frac{f_i}{\sqrt{2\pi\sigma_i^2}} \exp -\frac{(V_T^{(k)} - V_{T,i})^2}{2\sigma_i^2} \quad (3.21)$$

Where i represents the components, i.e., $i = 1, 2, 3$, f_i represents the fraction, $V_{T,i}$ represents the mean rotational velocity, σ_i represents velocity dispersion, and V_T^k rotational velocity of the k^{th} star.

From Bayes' theorem, we can write:

$$p(\theta/D) \propto p(D|\theta) p(\theta) \quad (3.22)$$

Our posterior distribution parameters can be defined based on Bayes' theorem which can be expressed in the following manner.

$$p(\theta_1, \theta_2, \theta_3 | V_T) \propto \prod_{k=1}^n \Sigma_{i=1}^3 p_i(V_T | \theta_i) p(\theta_1, \theta_2, \theta_3) \quad (3.23)$$

Where, $\theta_i = (f_i, V_{T,i}, \sigma_i)$ are the parameters vector of i^{th} components, k represents the star and n is a total number of stars.

The first component to find the posterior distribution is a likelihood function which is given in Eq. 3.23 for this case and the second component is a prior distribution. The prior distribution can be defined by using knowledge available from past or previous study. So, in our case we have used the prior similar to that of Tian et al. (2019) [6]. Prior used are: $0 < f_1 < 1$, $0 < f_2 < 1$, $0 < f_1 + f_2 < 1$, $-100 < V_{T,1} < 100$, $100 < V_{T,2} < 300$, $-200 < V_{T,3} < 0$, $0 < \sigma_{T,1} < 200$, $0 < \sigma_{T,2} < 200$ and $0 < \sigma_{T,3} < 200$. It should be noted that here $f_1 + f_2 + f_3 = 1$ and f_3 is not a free parameter because $f_3 = 1 - f_1 - f_2$.

After defining the likelihood function and prior distribution, our task is quite straightforward. To run the MCMC, we use a tool emcee [28]. For this, we define the 50 walkers each of dimension 8 and used 5000 burn-in. Once execution of MCMC complete, we choose the median value of samples as a best fit and difference of 16th and 84th percentile as lower and upper error of best fit.

3.2.4 Determination of Velocity Anisotropy (β)

To determine the velocity anisotropy, we initially compute the velocity of stars in a spherical coordinate. After computing the velocity in spherical coordinates, we create the binning of the stars based on

their galactocentric radii. After dividing them in group, we determine the velocity distribution of each group, i.e., σ_r : dispersion of radial velocity v_r , σ_θ : dispersion of a polar velocity and σ_ϕ : dispersion of azimuthal velocity. After calculating all these components, we are able to determine the velocity anisotropy. It should be noted that all the measurement over here is done using the spherical coordinate.

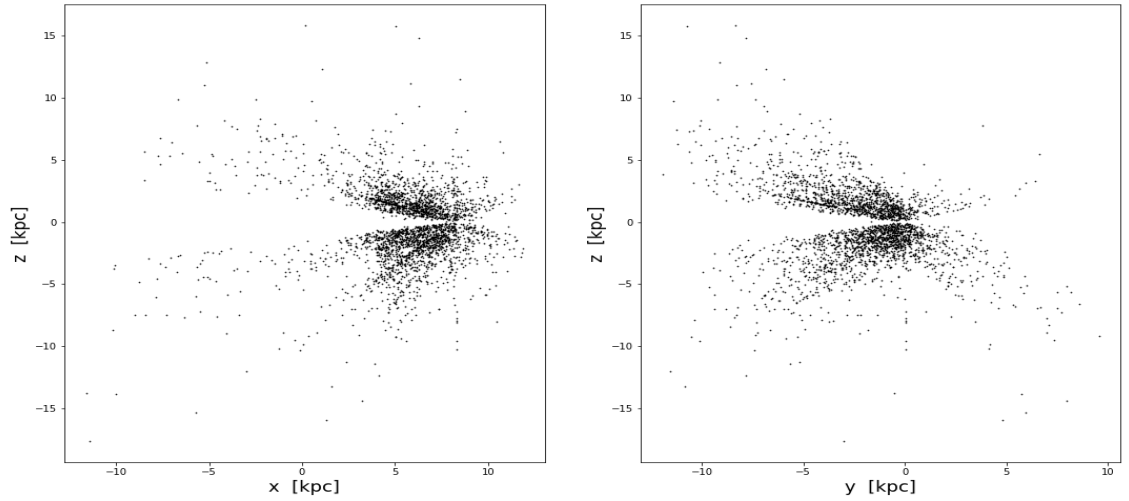


Figure 3.3: Spatial distribution of position of K-giant stars in Galactocentric cartesian coordinate system. Left panel: The distribution of K-giant stars in $z - x$ plane and at center of $z = 0.025$ kpc and $x = R_\odot$. Right panel: The distribution of K-giant stars in $y - x$ plane.

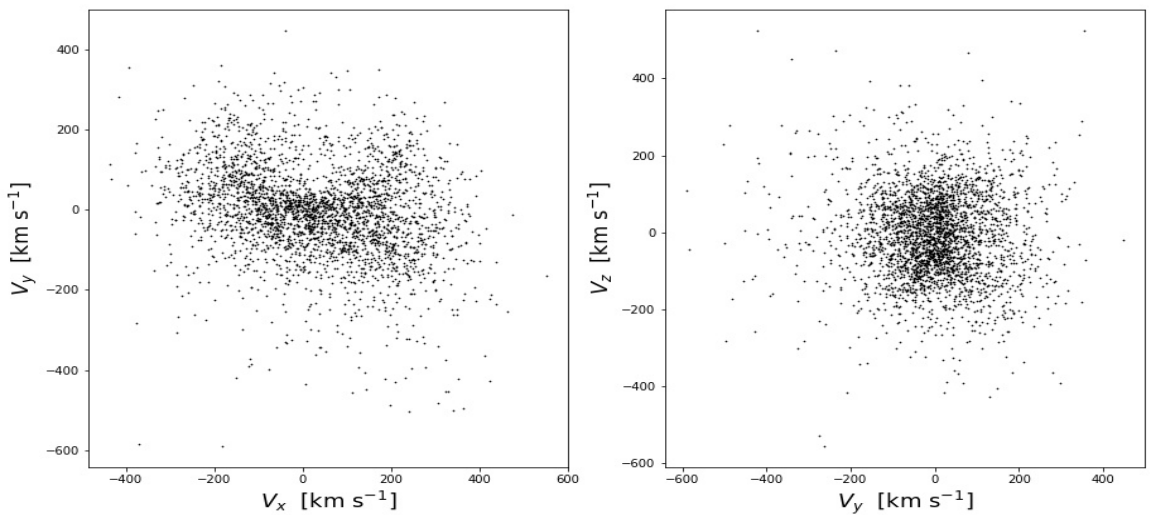


Figure 3.4: Distribution of velocity of the K-giant stars in Galactocentric cartesian coordinate system.

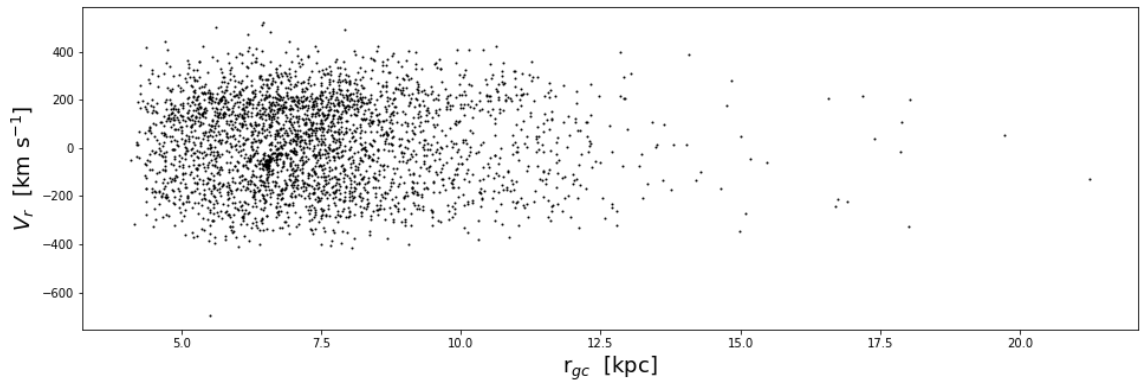


Figure 3.5: The galactocentric radius r_{gc} versus radial velocity V_r .

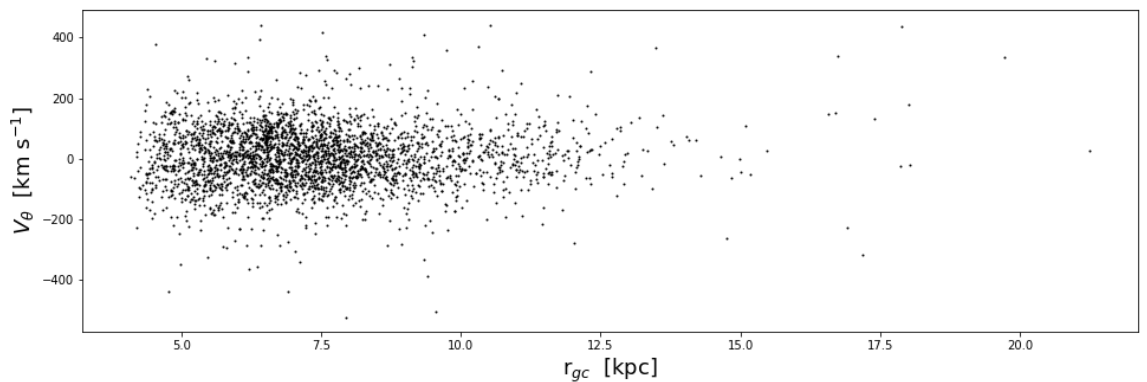


Figure 3.6: The galactocentric radius r_{gc} versus polar velocity V_θ .

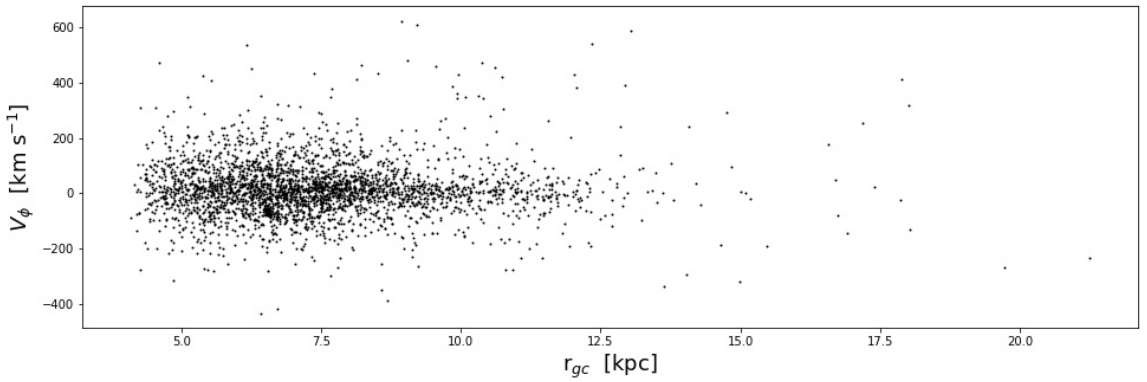


Figure 3.7: The galactocentric radius r_{gc} versus azimuthal velocity V_ϕ .

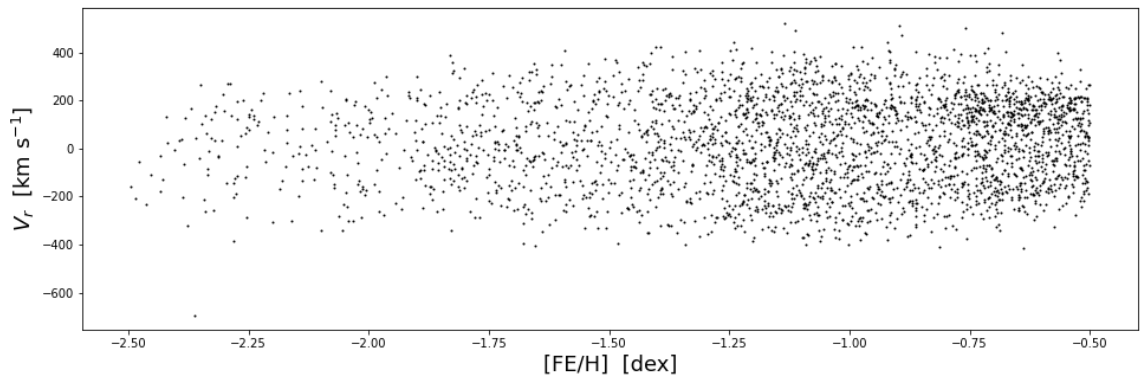


Figure 3.8: The metallicity [Fe/H] versus radial velocity V_r .

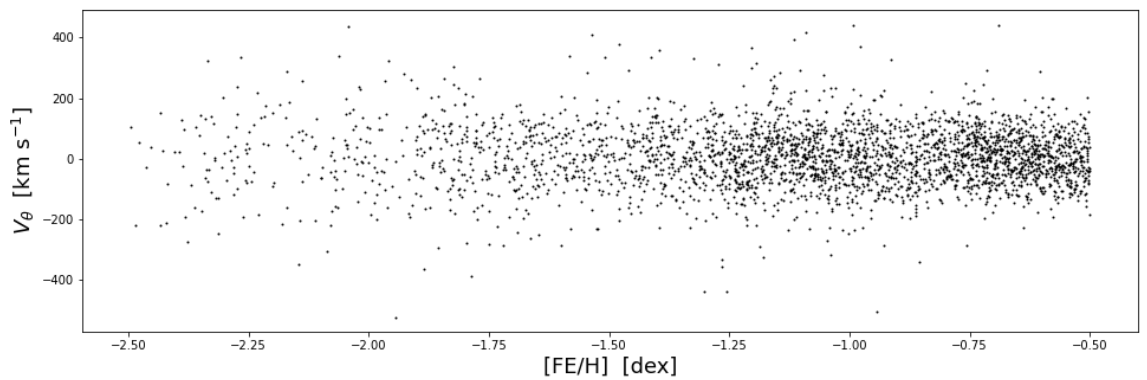


Figure 3.9: The metallicity [Fe/H] versus polar velocity V_θ .

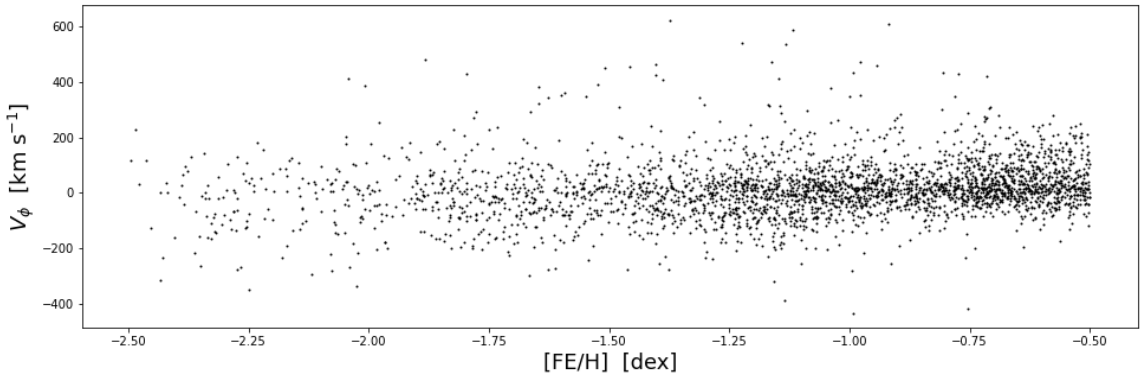


Figure 3.10: The metallicity [Fe/H] versus azimuthal velocity V_ϕ .

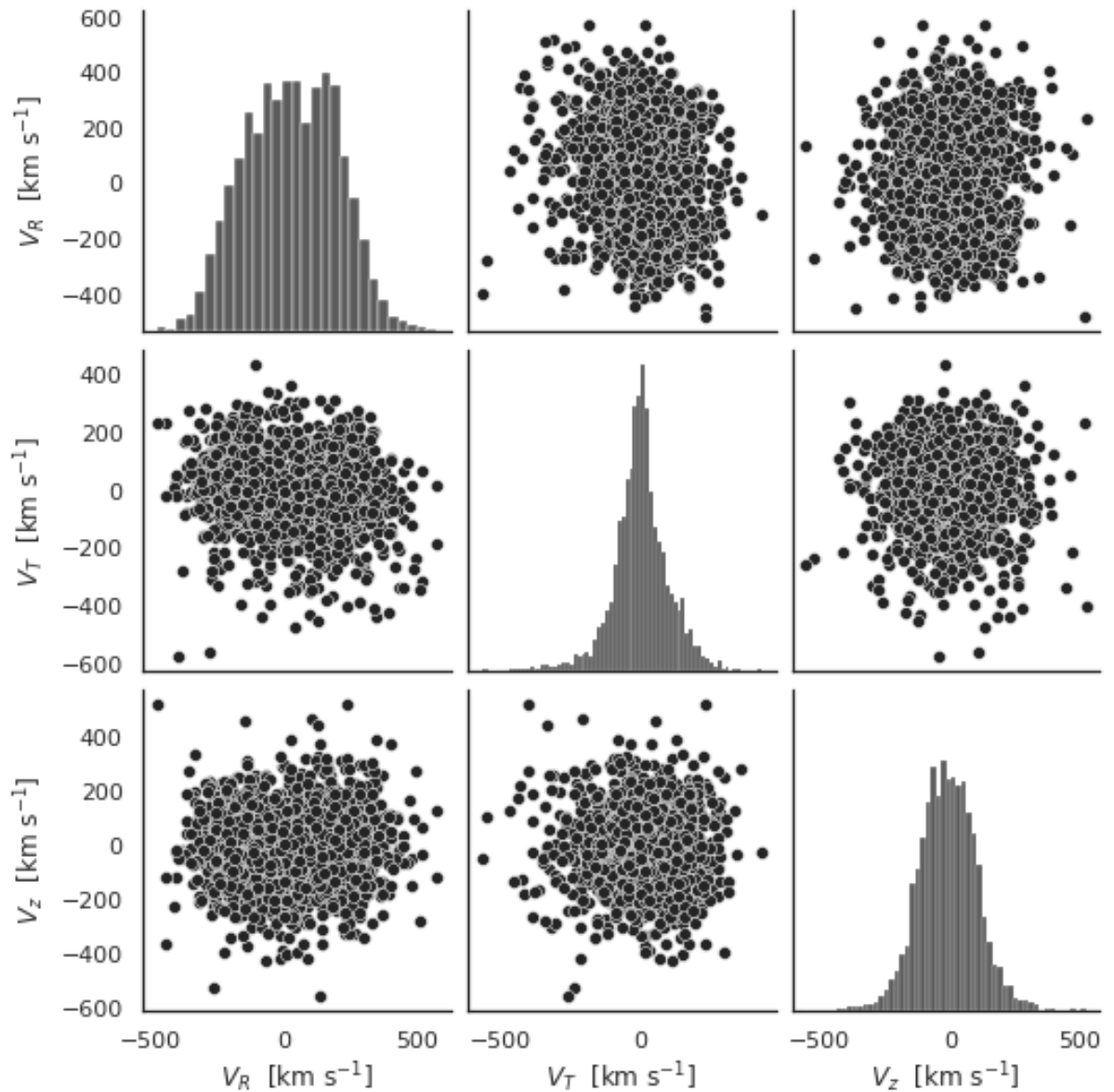


Figure 3.11: The distributions of the velocity of K-giant stars in a cylindrical coordinate system. Along the diagonal, the distribution of cylindrical velocity components in the histogram and in off-diagonal, the scattering plot between various cylindrical velocity-components.

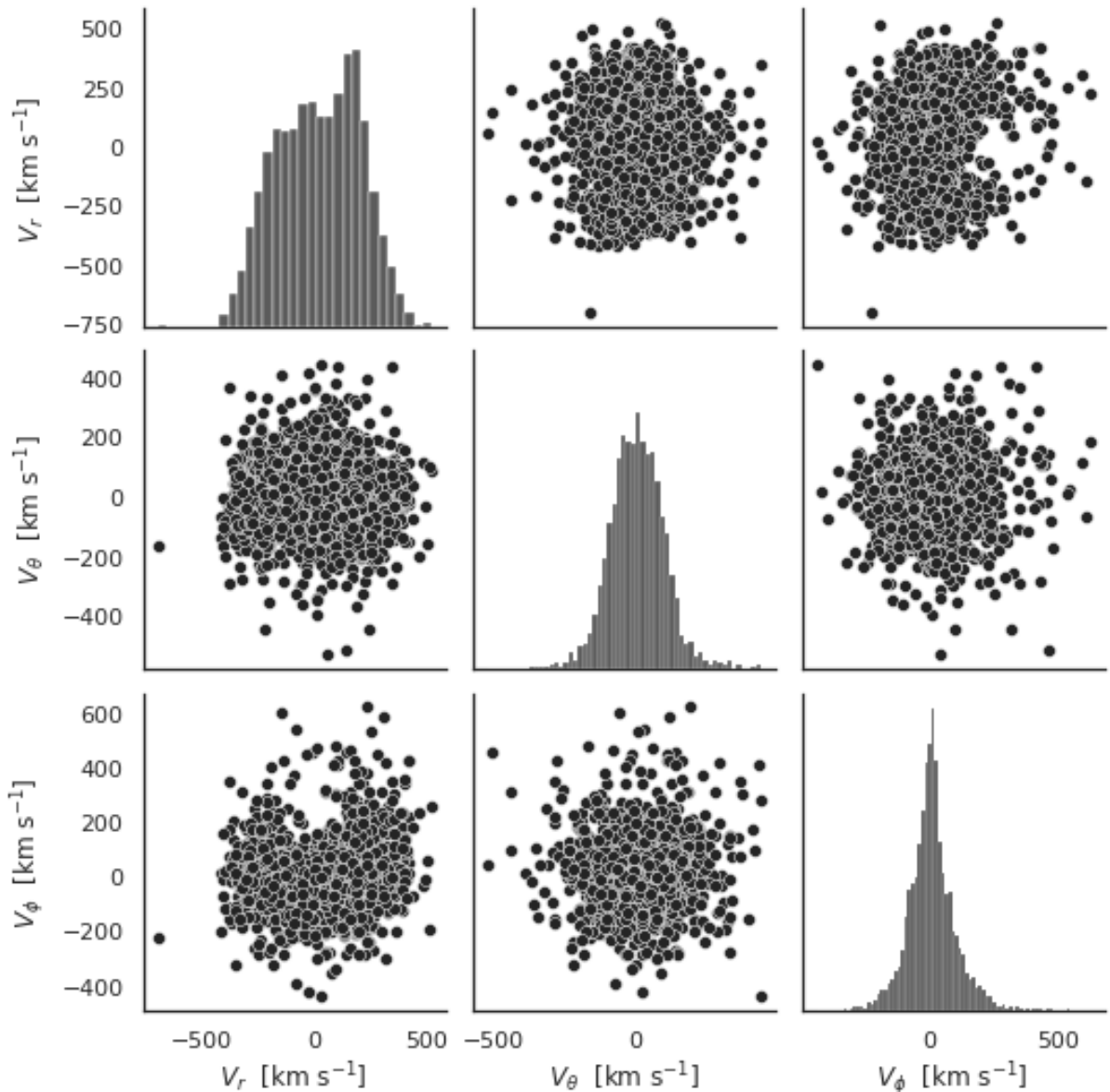


Figure 3.12: The distributions of the velocity of K-giant stars in a spherical coordinate system. Along the diagonal, the distribution of spherical velocity components in the histogram and in off-diagonal, the scattering plot between various spherical velocity-components.

Chapter 4

Result & Discussion

4.1 Result

4.1.1 Rotational Velocity

In Fig. 4.2, we have a corner plot representing the posterior distribution of our sample. This corner plot is a result of sampling done by MCMC over a range of parameter values. From the figure, we have obtained the best fit values for the different parameters that have given in likelihood function, and error for each parameter that is evaluated by the difference of median with 16th and 84th percentile of samples. In the corner plot, the blue line represents the median value of samples that we have taken as best fit.

In Fig. 4.2, we have values of mean and standard deviation for three Gaussian components along with that these are values of fractions f_i which we have assumed earlier in likelihood.

From this corner plot, we find $f_1 = 0.650^{+0.042}_{-0.041}$, $V_{T,1} = -5^{+3}_{-3}$ km s⁻¹ and $\sigma_{T,1} = 55^{+3}_{-3}$ km s⁻¹, this value exhibits that this region is nearly steady and exhibits very small retrograde motion. These facts indicate that this region is an inner halo as a similar small retrograde-motion for

the inner halo that obtained by Kordopatis *et al.* (2013) ($v_\phi = -1 \pm 11$ km s $^{-1}$, $\sigma_\phi = 96 \pm 7$ km s $^{-1}$) [29] and Carollo *et al.* (2010) [27] ($v_\phi = -5$ km s $^{-1}$, $\sigma_\phi = 87$ km s $^{-1}$). Importantly, Kafle *et al.* [7] also have proposed similar retrograde motion for inner halo.

From Fig. 4.2 we obtain $f_2 = 0.121^{+0.05}_{-0.03}$, $V_{T,2} = 135^{+14}_{-20}$ km s $^{-1}$ and $\sigma_{T,2} = 59^{+13}_{-12}$ km s $^{-1}$. We can see this region shows a prograde motion with large speed. This region is metal weak thick disk (MWTD) ; this is consistent with what has been found in previous by Carollo *et al.* (2010) ($v_\phi = 125 \pm 4$ km s $^{-1}$, $\sigma_\phi = 40 \pm 3$ km s $^{-1}$) [27], Kordopatis *et al.* ($v_\phi = 123 \pm 16$ km s $^{-1}$, $\sigma_\phi = 61 \pm 12$ km s $^{-1}$) [29] for MWTD and further Carollo *et al.* (2010) also mentioned that MWTD will have v_ϕ in between 100 km/s to 150 km/s [27].

For f_3 , we evaluate as $f_3 = 1 - f_1 - f_2$ so we get $f_3 = 0.229$ and other value are obtained using the fig 4.2. So, we get $V_{T,3} = -41^{+15}_{-19}$ km s $^{-1}$ and $\sigma_{T,3} = 153^{+7}_{-7}$ km s $^{-1}$ that similar pattern of results was obtained by Carollo *et al.* (2007) [30] for outer halo. So, the third component of our result represents the outer halo.

In Fig. 4.1, we can see the main plot of all the samples and then the plot of the different components determined in the corner plots which are denoted by dotted lines. In this figure, the tail region on left with a small bump that represents the third component or outer halo with large retrograde motion; in middle,a peak that represents the third component that is the inner halo and finally, a small peak on the left region that represents the second component or MWTD. So from all these facts, we can conclude our data is composed of three regions or components that show properties different from one another.

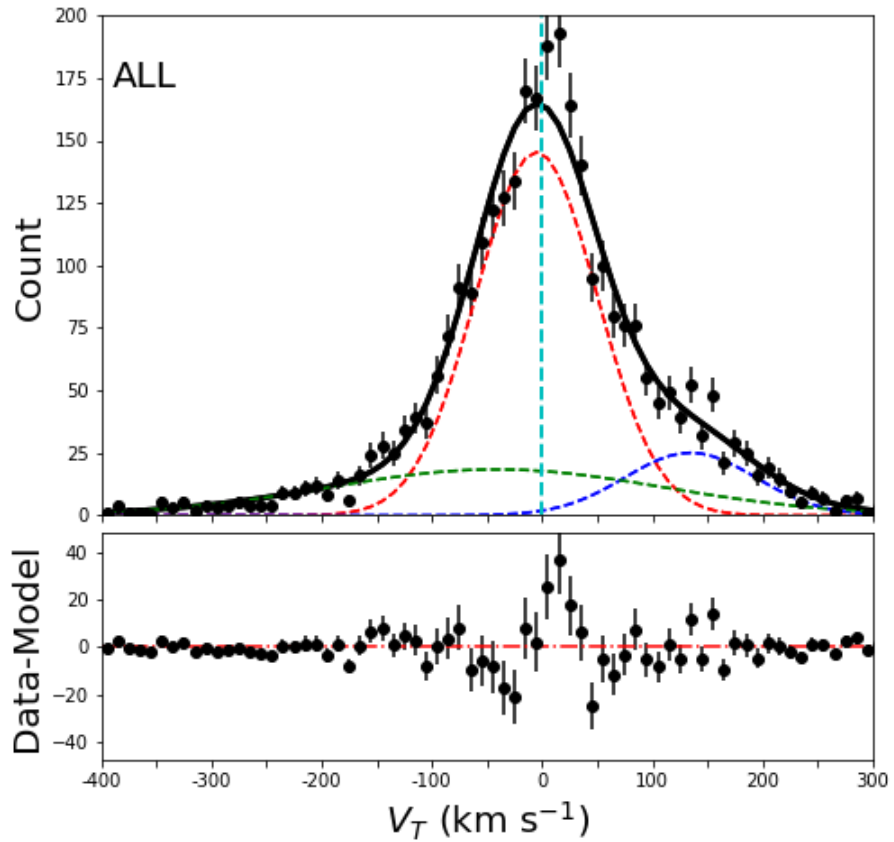


Figure 4.1: The plot of distribution of azimuthal velocity (V_T) with an error bar generated using Poisson distribution. The dark black line represents the entire sample, the red dash line represents the first component, the blue dash line represents the second component and the green dash line represents the third component.

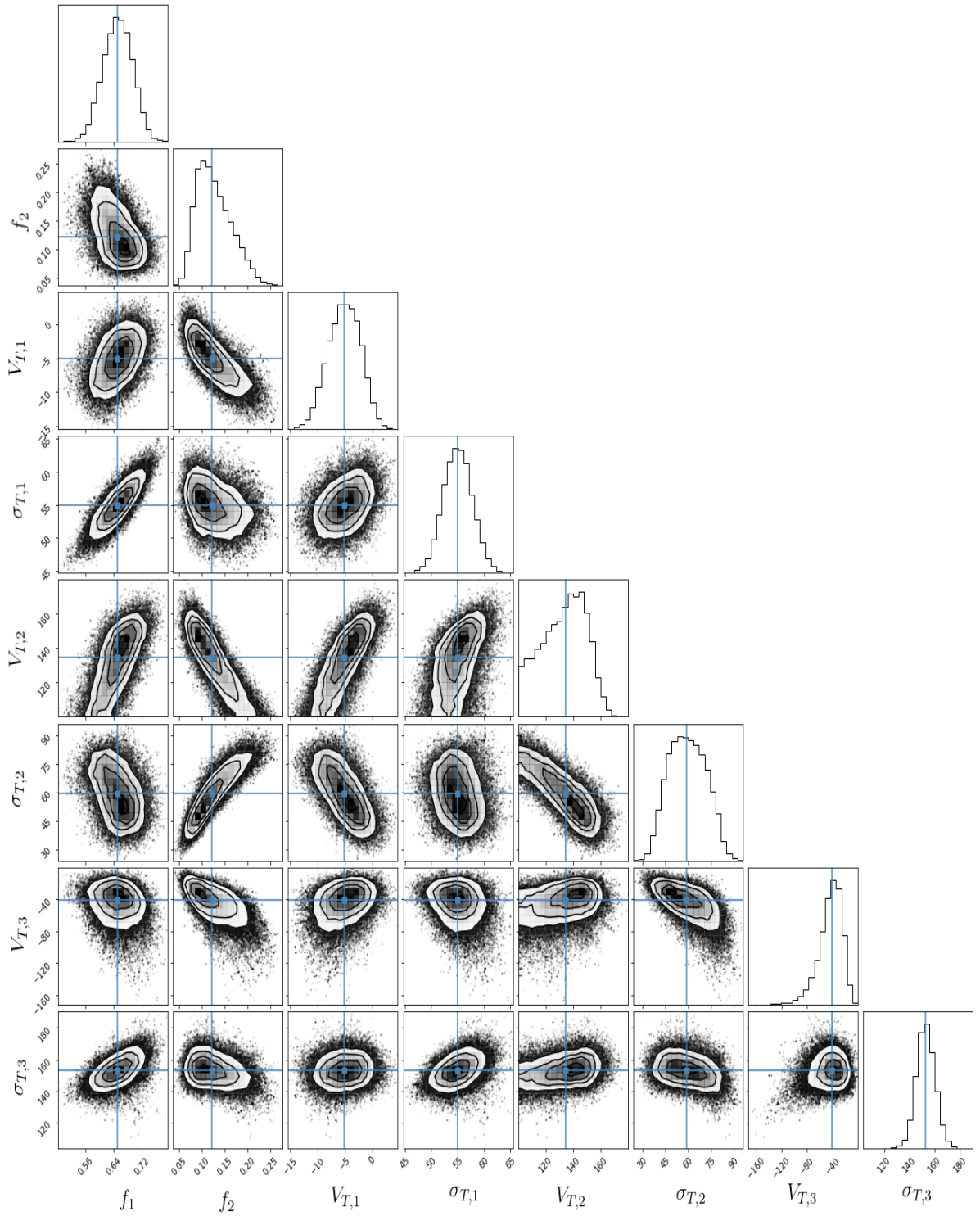


Figure 4.2: The result of MCMC is shown in the corner plot. The corner plot shows the correlation between any two parameters. The blue line indicates the median value of samples which we have taken as the best fit. 1σ , 2σ and 3σ counters shows the joint posterior probability distribution of our parameters (θ_i 's) for K-giant stars. The histogram represents one-dimensional marginalized posterior distribution.

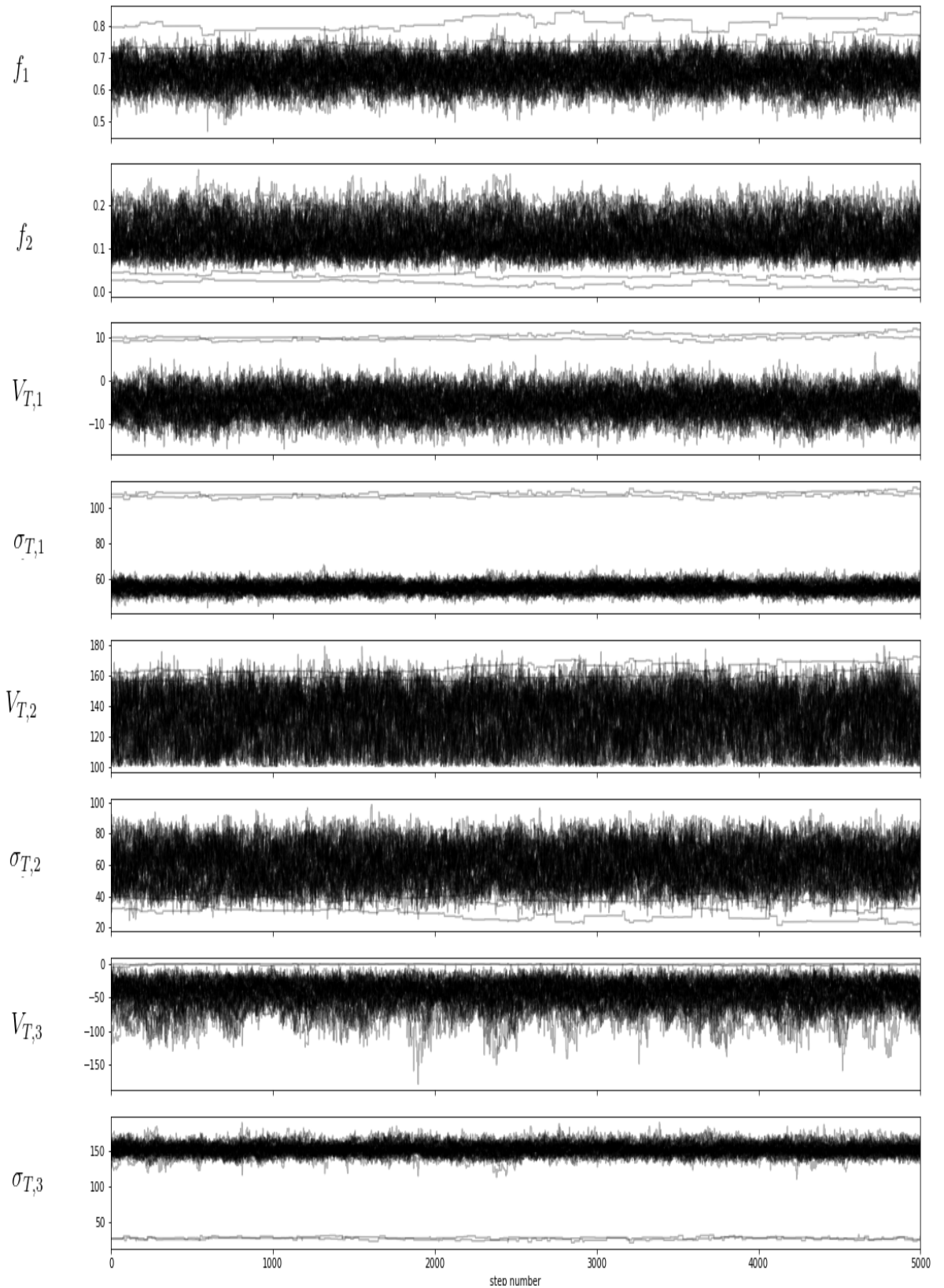


Figure 4.3: Position of our walker as a function of the number of steps (for all 3081 K-giant stars). This plot also depicts more about walkers having entire parameter space of posterior distribution. This plot represents the random walk followed by the walkers.

4.1.2 Velocity Anisotropy

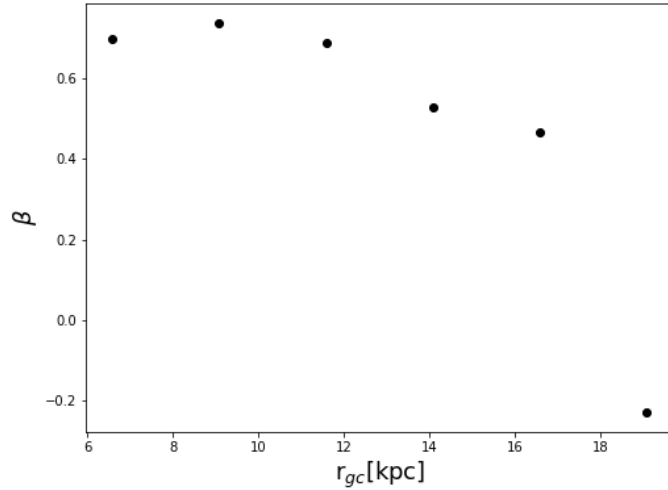


Figure 4.4: The plot of velocity anisotropy(β) as a function of the galactocentric radius, here we have binned star at 2.5 kpc galactocentric radius.

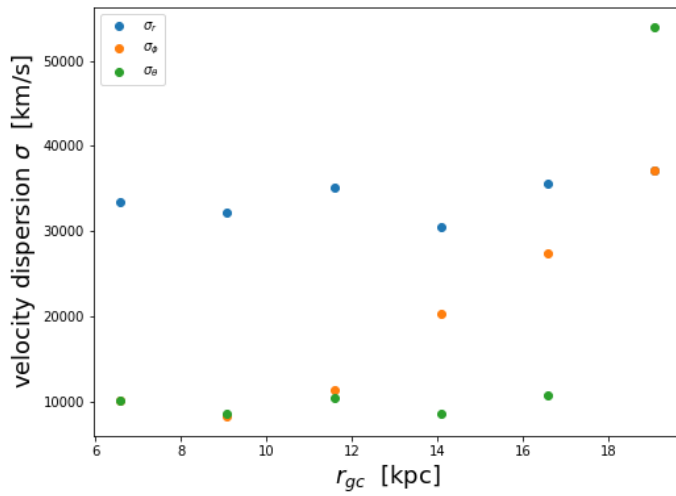


Figure 4.5: Plot of the velocity dispersions ($\sigma_r, \sigma_\theta, \sigma_\phi$) with the galactocentric radius binned at 2.5 kpc.

By analyzing the Fig. 4.4 we find beta decreases as distance increases which is similar to that observed by kafle *et al.* (2013) [31] and also by

Deason *et al.* (2011) [32]. In other words, the orbit of the star becomes more tangential as distance increases. If we consider the entire sample as a one and measure the anisotropy then we get $\beta = 0.48$, which shows that the overall orbit of the K-giant stars is radial.

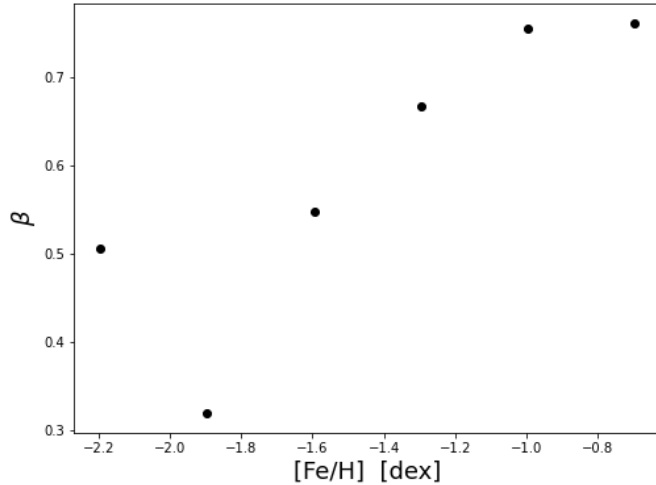


Figure 4.6: Plot of velocity anisotropy (β) as a function of the metallicity ([Fe/H]). Here we have binned the star in 0.3 dex metallicity.

Further, to observe the effect of the metallicity on β , we divide our entire sample according to their metallicity (i.e we bin star with bin size = 0.3 dex) and measure the anisotropy of each bin which is shown in 4.6. From 4.6 we can observe there is no significant variation of β with metallicity. We obtain all beta to be positive on binning according to metallicity so all of them have a radially biased orbit.

4.1.3 Energy and Angular Momentum

We evaluate the total energy of stars (i.e sum of kinetic energy and potential energy) using the built-in function of galpy [26]. We evaluate the angular momentum of the stars using Eq. 2.35. Then, the plotted the energy versus momentum plot as shown in Fig. 4.1.3.

Source id	α (deg)	δ (deg)	\bar{w} (mas)	μ_α (mas yr $^{-1}$)	μ_δ (mas yr $^{-1}$)	v_{rad} (km s $^{-1}$)	E (km s $^{-1}$) 2	L (kpc kms $^{-1}$)	L_z (kpc kms $^{-1}$)
4.667213730748377e+18	52.357	-69.554	0.198	9.494	1.747	263.88	-165699.573	237.101	481.061
4.670295283883987e+18	51.969	-68.577	0.07	3.123	-0.684	214.39	-168455.924	650.124	796.641
4.775063383207773e+18	67.977	-57.675	0.63	10.392	-12.724	211.99	-171002.376	544.928	716.825
4.760221762939506e+18	82.824	-58.168	0.718	22.106	21.164	135.32	-172482.39	924.515	1094.349
4.760132904360198e+18	82.393	-58.678	0.18	4.704	-2.472	186.77	-174835.061	42.211	758.993
4.763290431173097e+18	81.048	-57.57	0.441	17.739	-1.437	190.88	-174562.697	537.699	753.781
4.766305670013543e+18	82.12	-57.464	0.165	4.133	-3.178	160.18	-173869.688	74.685	928.423
5.482522940142496e+18	92.356	-59.653	0.685	16.939	-9.099	319.42	-172821.183	897.712	-259.985
5.494630315510644e+18	92.786	-58.82	0.166	4.87	-0.909	272.38	-176558.896	603.368	96.927
5.494846919301524e+18	93.005	-58.298	0.14	4.733	0.209	239.67	-177479.987	562.761	280.507

Table 4.1: Source id, right ascension, declination, parallax, proper motions, radial velocity, energy, angular momentum and angular momentum along z - direction for 10 K-giant stars out of 3081 K-giant stars on our data.

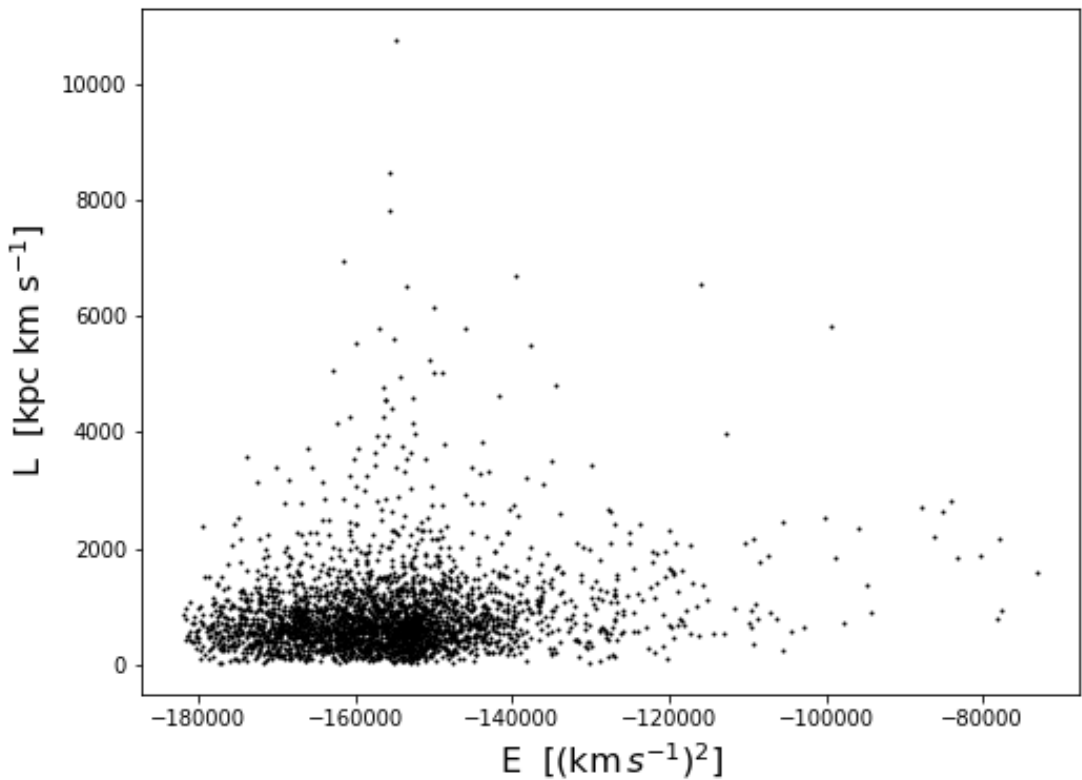


Figure 4.7: Energy vs total angular momentum plot of our 3081 K-giant stars where potential is evaluated using McMillian17 of galpy. [23].

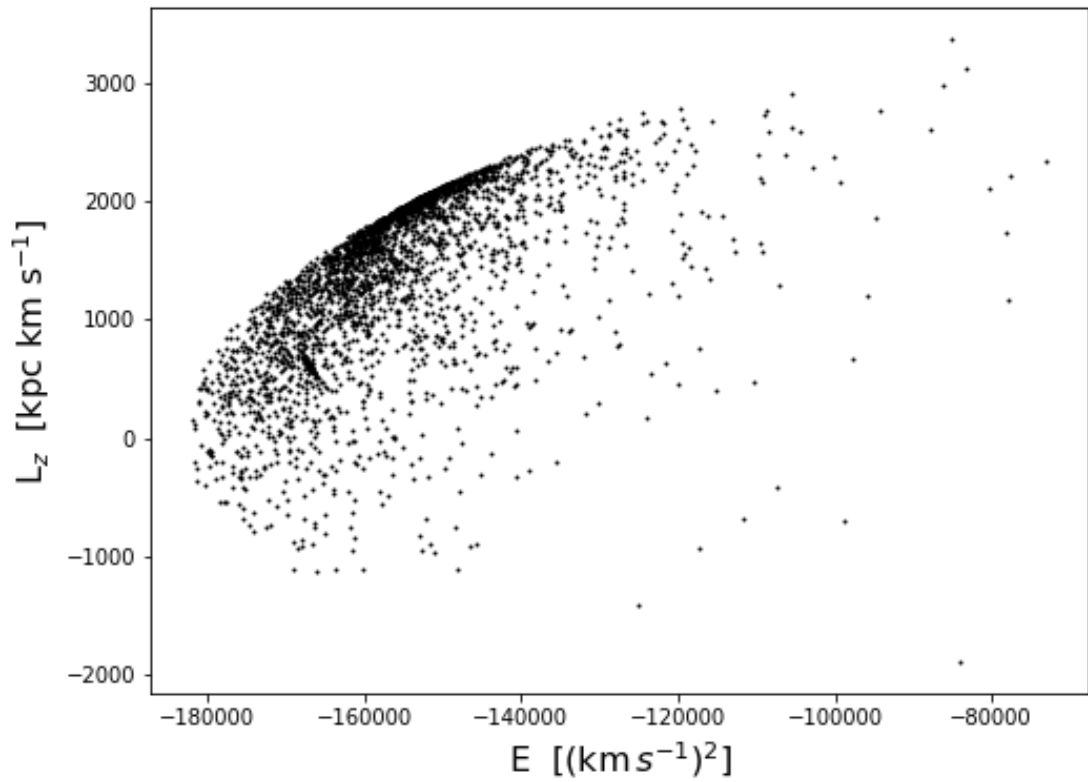


Figure 4.8: Energy vs z-component of angular momentum plot of our 3081 K-giant stars where potential is evaluated using McMillian17 of galpy. [23].

4.2 Discussion

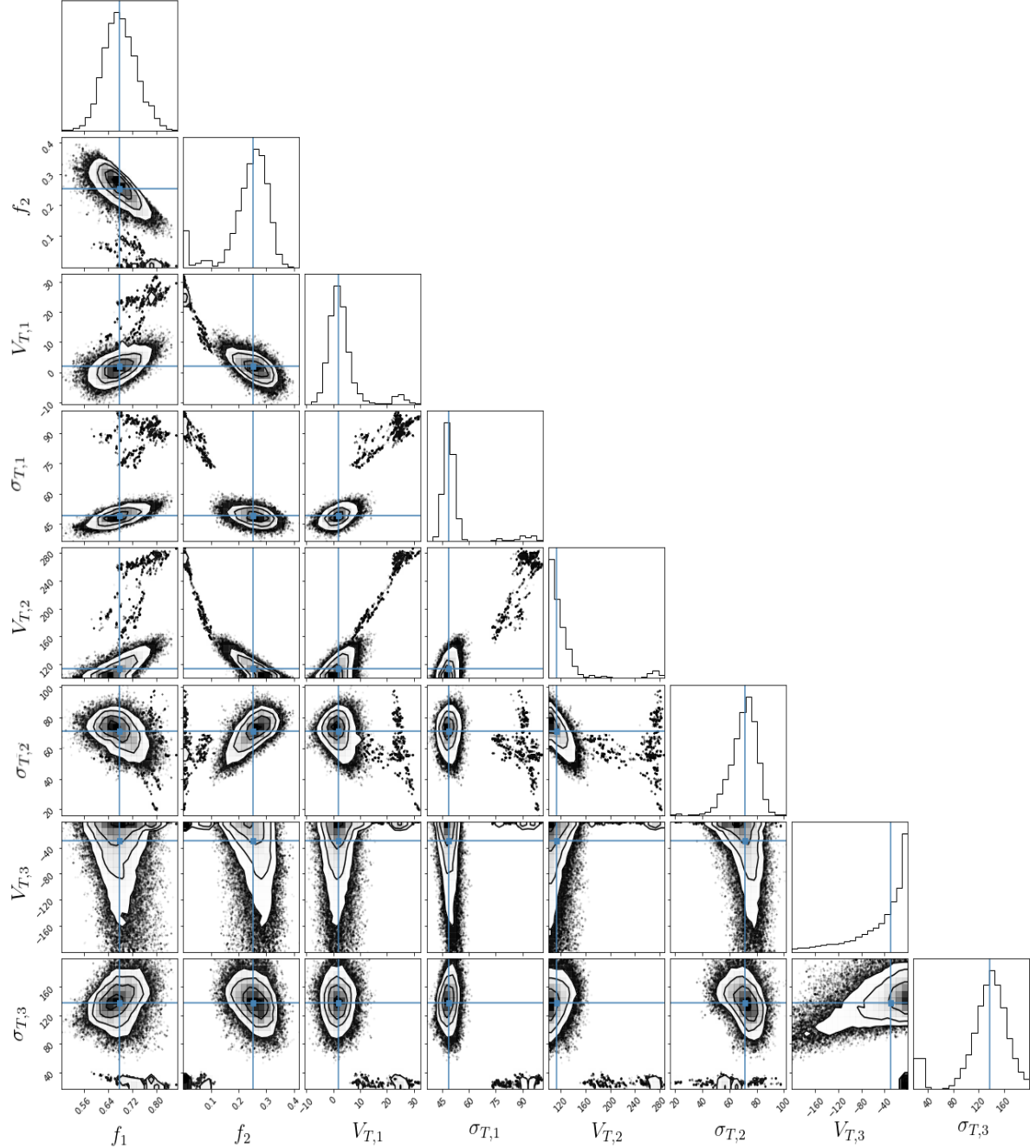


Figure 4.9: The result of MCMC for K-giant stars with metallicity $-0.9 \text{ dex} < [\text{Fe}/\text{H}] < -0.5 \text{ dex}$ is shown in the corner plot. Corner plot shows the correlation between any two parameters. The blue line indicate the median value of samples which we have taken as a best fit. 1σ , 2σ and 3σ counters shows the joint posterior probability distribution of our parameters (θ_i 's) for K-giant stars. The histogram represent one dimensional marginalize posterior distribution.

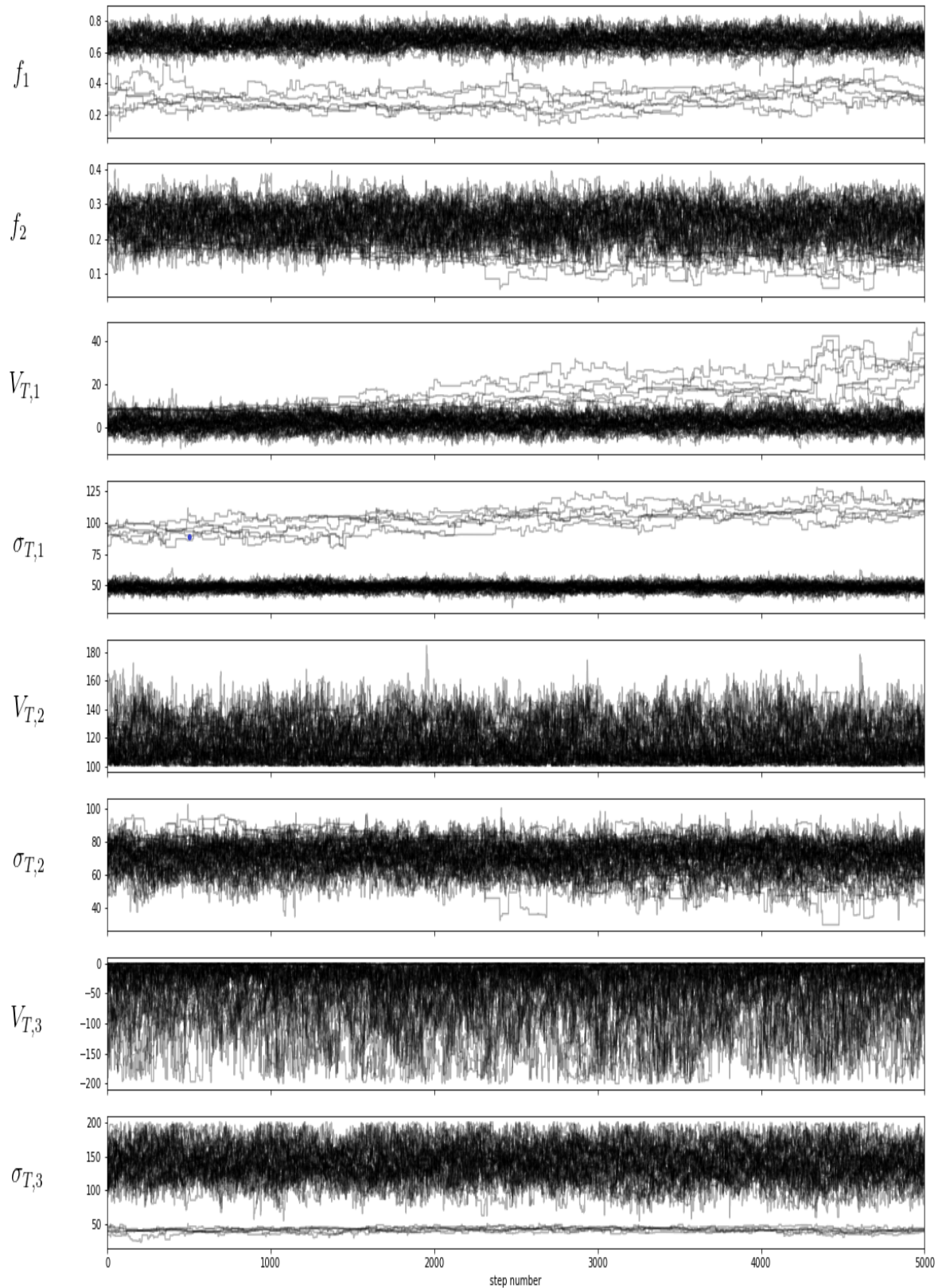


Figure 4.10: Position of our walkers as a function of number of steps (for all K-giant stars with metallicity $-0.9 \text{ dex} < [\text{Fe}/\text{H}] < -0.5 \text{ dex}$).

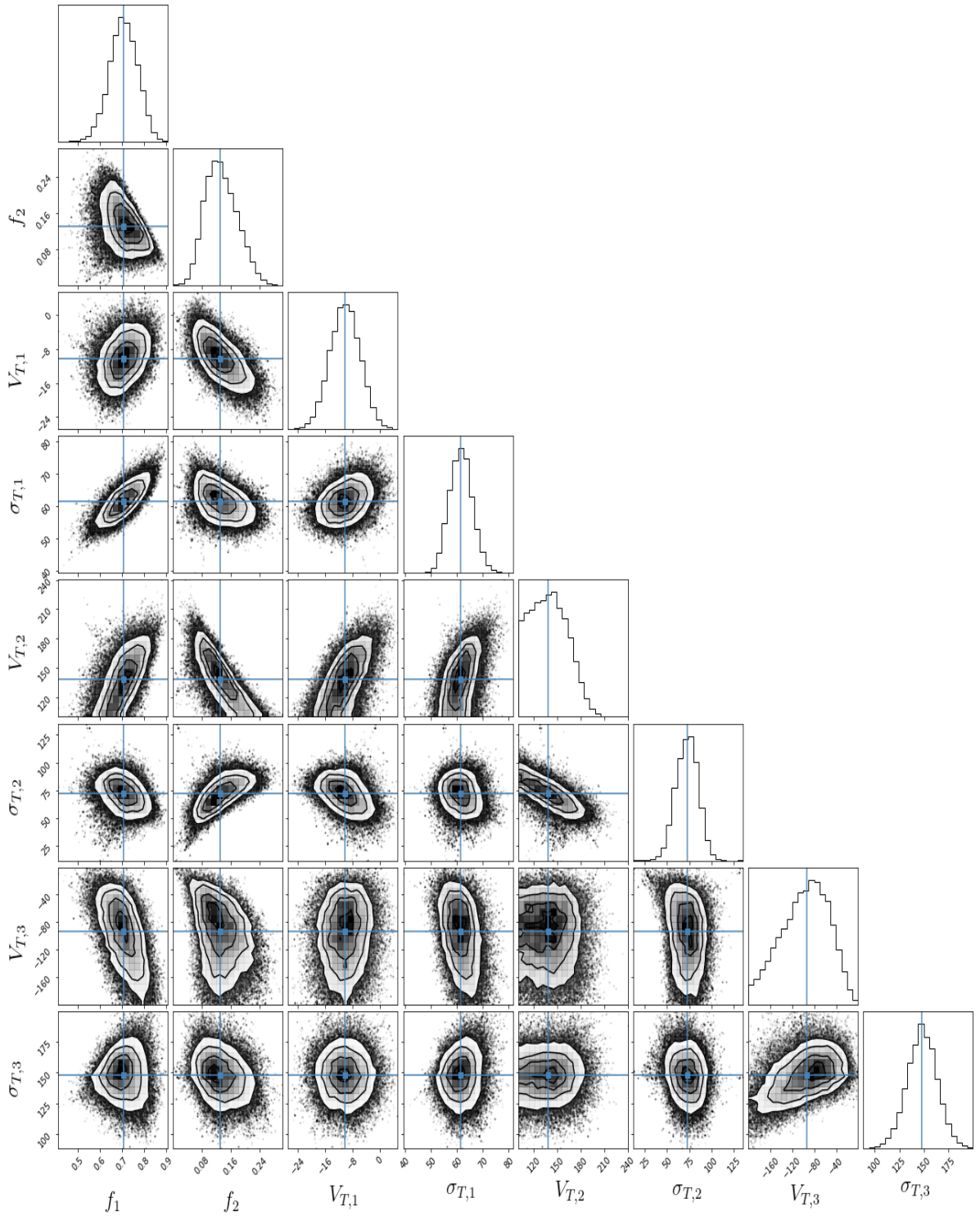


Figure 4.11: The result of MCMC for K-giant stars with metallicity $-1.3 \text{ dex} < [\text{Fe}/\text{H}] < -0.9 \text{ dex}$ is shown in the corner plot. Corner plot shows the correlation between any two parameters. The blue line indicate the median value of samples which we have taken as a best fit. 1σ , 2σ and 3σ counters shows the joint posterior probability distribution of our parameters (θ_i 's) for K-giant stars. The histogram represent one dimensional marginalized posterior distribution.

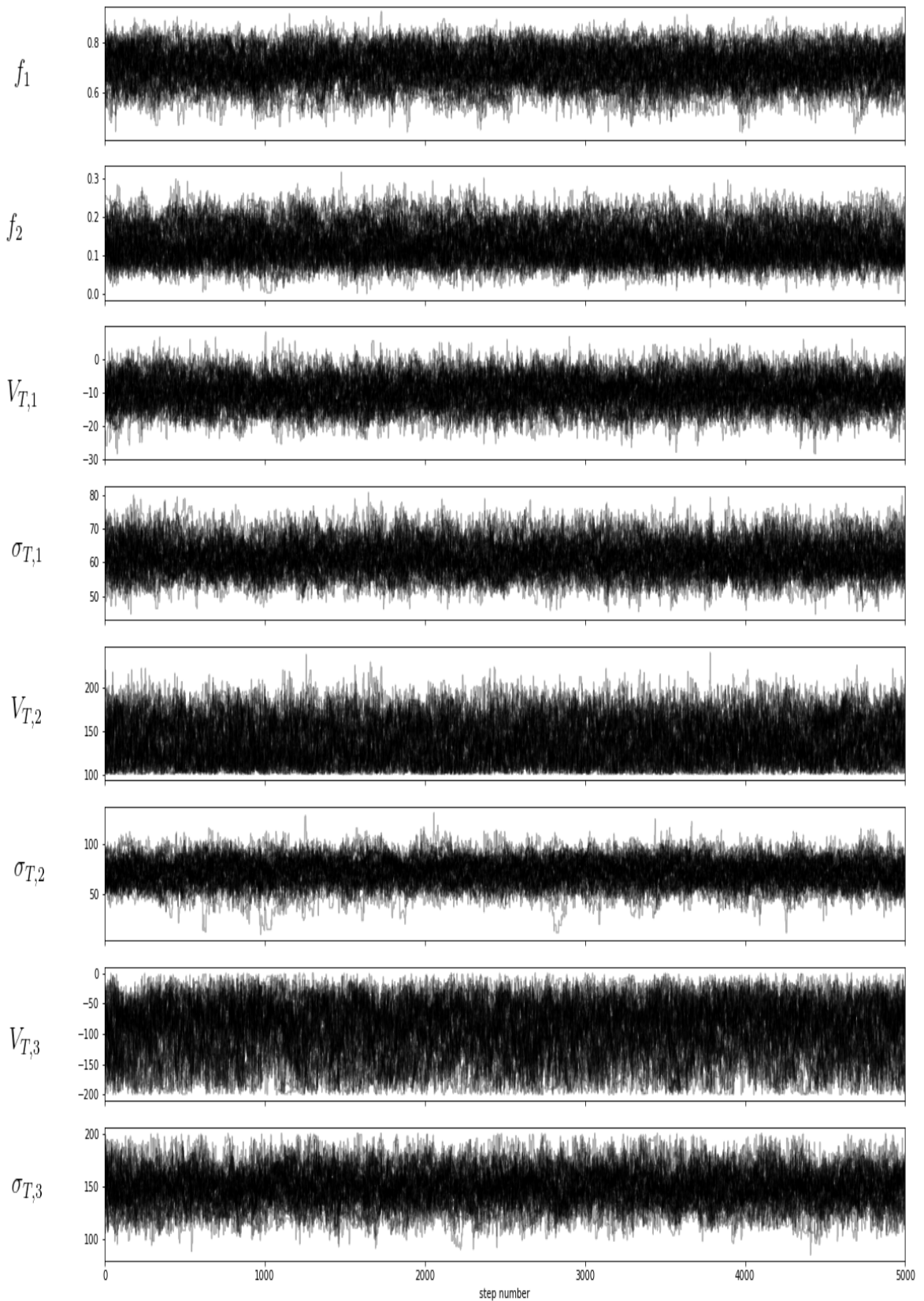


Figure 4.12: Position of our walkers as a function of number of steps (for all K-giant stars with metallicity $-1.3 \text{ dex} < [\text{Fe}/\text{H}] < -0.9 \text{ dex}$).

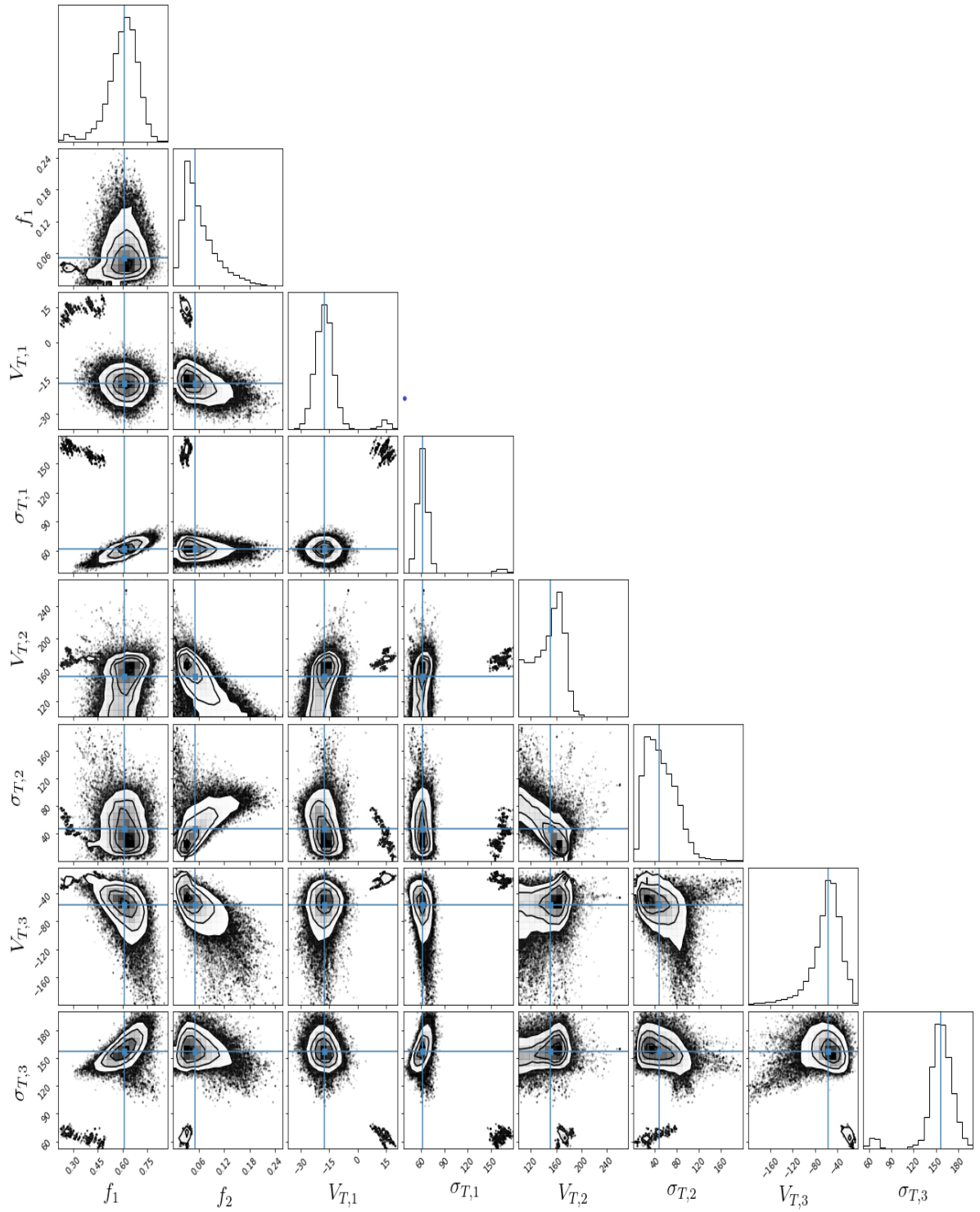


Figure 4.13: The result of MCMC for K-giant stars with metallicity $-2.5 \text{ dex} < [\text{Fe}/\text{H}] < -1.3 \text{ dex}$ is shown in the corner plot. Corner plot shows the correlation between any two parameters. The blue line indicate the median value of samples which we have taken as a best fit. 1σ , 2σ and 3σ counters shows the joint posterior probability distribution of our parameters (θ_i 's) for K-giant stars. The histogram represent one dimensional marginalize posterior distribution.

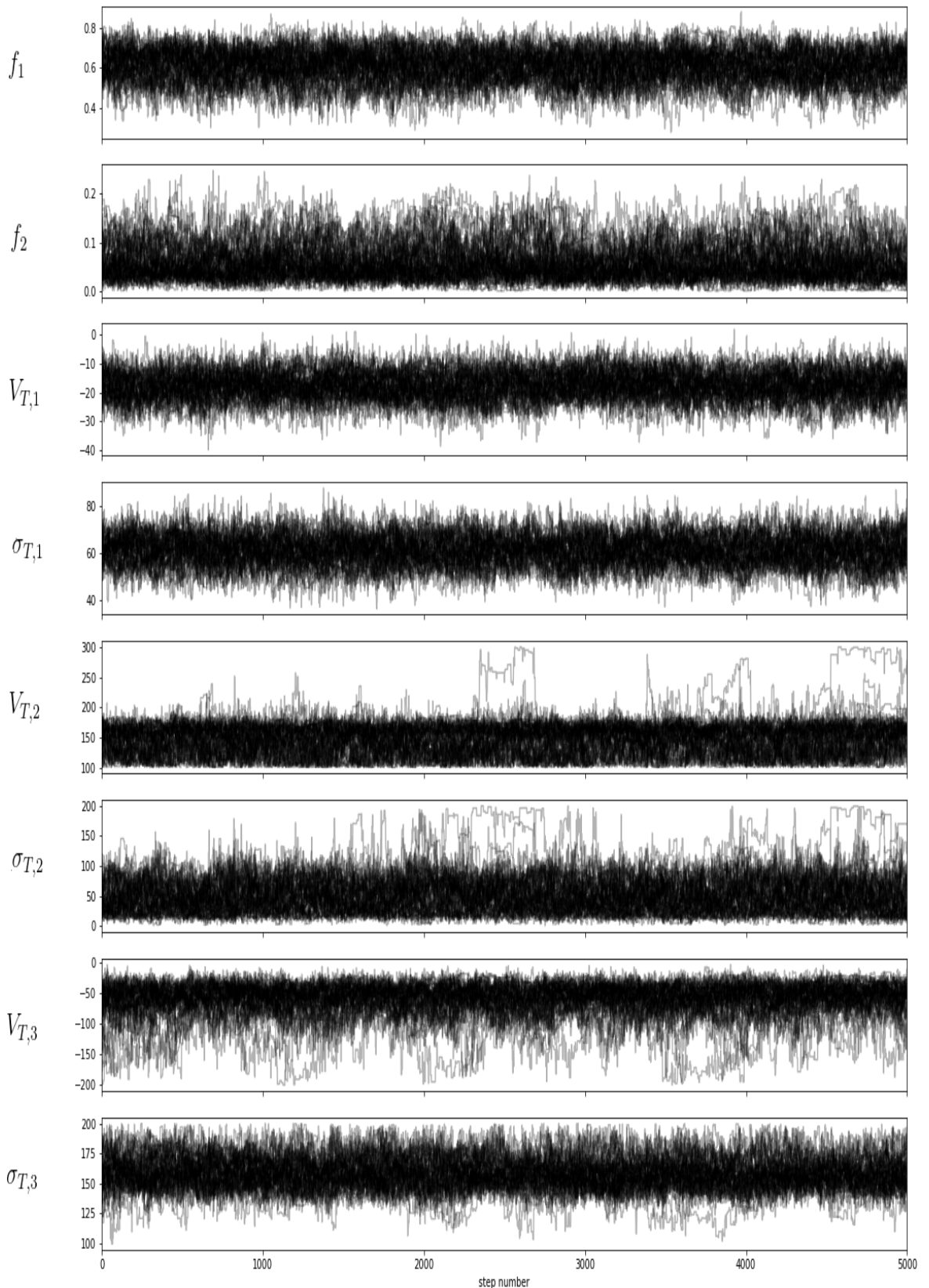


Figure 4.14: Position of our walkers as a function of number of steps (for all K-giant stars halo stars with metallicity $-2.5 \text{ dex} < [\text{Fe}/\text{H}] < -1.3 \text{ dex}$).

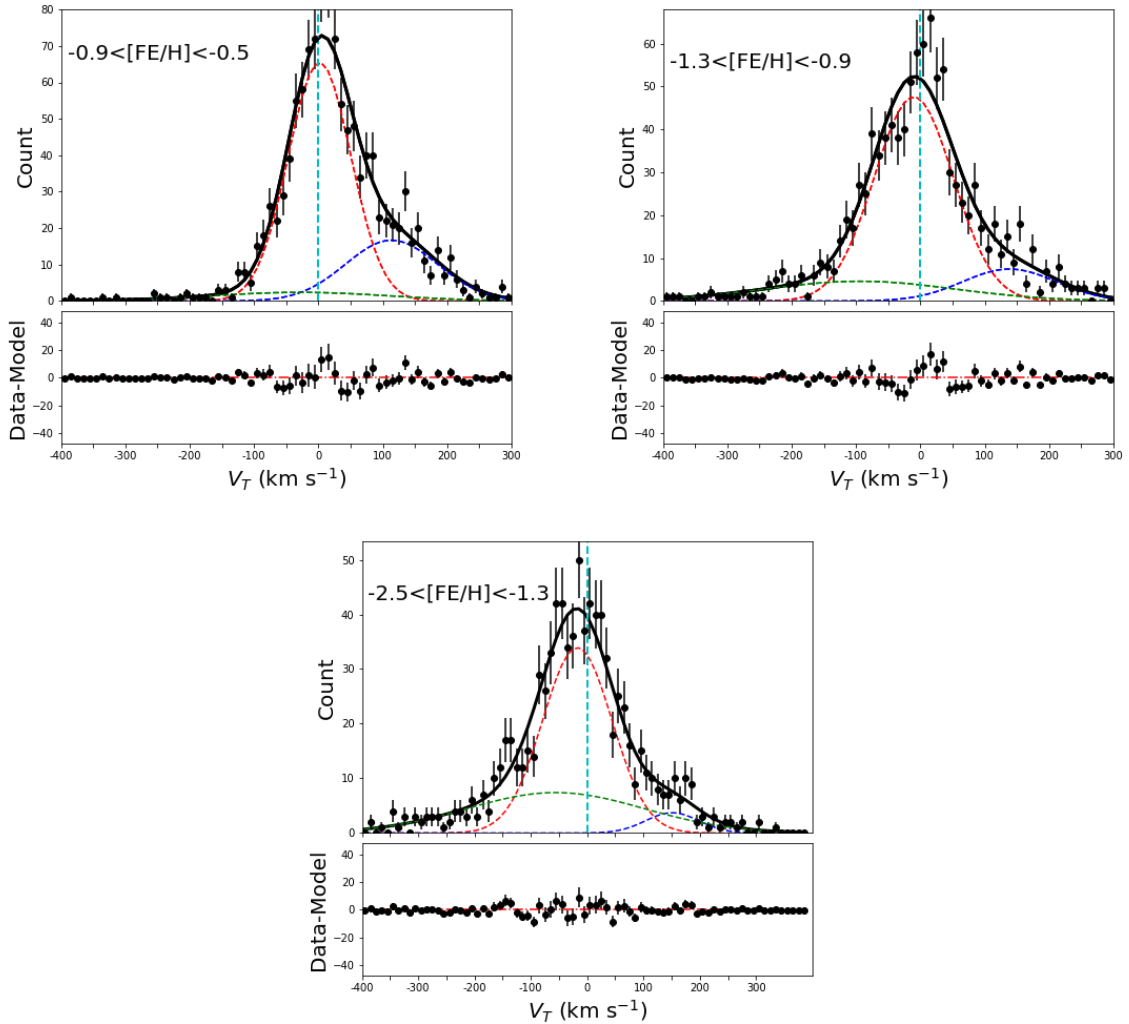


Figure 4.15: Distribution of the azimuthal velocity V_T of 3081 K-giant stars divided according to metallicity, first being the metal richest and third being the metal poorest K-giant stars in our sample. Here error is generated using the Poisson distribution.

To determine the effect of metallicity on the rotational velocity, we have divided the entire sample of K-giant stars into 3 groups depending upon their metallicity. After dividing them into three groups, we have determined the rotational velocity for each group independently by fitting three Gaussian components. The result obtained for different groups are as follow:

1. First group consist of 1181 metal rich K-giant stars with metallicity in between $-0.9 < [\text{Fe}/\text{H}] < -0.5$, on fitting three component gaussian to it we get:

$$f_1 = 0.678_{-0.049}^{+0.056}, f_2 = 0.253_{-0.063}^{+0.046}, f_3 = 0.069, V_{T,1} = 2_{-1}^{+4} \text{ km s}^{-1}, \\ \sigma_{T,1} = 49_{-3}^{+4} \text{ km s}^{-1}, V_{T,2} = 114_{-10}^{+20} \text{ km s}^{-1}, \sigma_{T,2} = 71_{-10}^{+8} \text{ km s}^{-1}, \\ V_{T,3} = -29_{-64}^{+24} \text{ km s}^{-1}, \sigma_{T,3} = 138_{-30}^{+23} \text{ km s}^{-1}.$$

The corner Fig. 4.9 represents the output of MCMC samples for this group.

2. The second group consists of 1039 K-giant stars with metallicity in between $-1.3 < [\text{Fe}/\text{H}] < -0.9$, on fitting three-component Gaussian to it we get the following results:

$$f_1 = 0.706_{-0.06}^{+0.06}, f_2 = 0.130_{-0.040}^{+0.049}, f_3 = 0.164, V_{T,1} = -10_{-4}^{+4} \text{ km s}^{-1}, \\ \sigma_{T,1} = 61_{-4}^{+4} \text{ km s}^{-1}, V_{T,2} = 138_{-25}^{+25} \text{ km s}^{-1}, \sigma_{T,2} = 72_{-12}^{+11} \text{ km s}^{-1}, \\ V_{T,3} = -94_{-49}^{+40} \text{ km s}^{-1}, \sigma_{T,3} = 148_{-15}^{+15} \text{ km s}^{-1}.$$

The corner plot 4.11 represents the output of MCMC samples for this group.

3. Third group consist of 1039 metal-poor K-giant stars with metallicity in between $-2.5 < [\text{Fe}/\text{H}] < -1.3$, on fitting three-component Gaussian to it we get:

$$f_1 = 0.611_{-0.091}^{+0.073}, f_2 = 0.094_{-0.023}^{+0.045}, f_3 = 0.295, V_{T,1} = -17_{-5}^{+5} \text{ km s}^{-1}, \\ \sigma_{T,1} = 62_{-6}^{+6} \text{ km s}^{-1}, V_{T,2} = 151_{-32}^{+8} \text{ km s}^{-1}, \sigma_{T,2} = 47_{-23}^{+31} \text{ km s}^{-1}, \\ V_{T,3} = -56_{-26}^{+18} \text{ km s}^{-1}, \sigma_{T,3} = 157_{-12}^{+13} \text{ km s}^{-1}.$$

The corner plot 4.13 represents the output of MCMC samples for this group.

So, on analyzing the rotational velocities of different metallicity group,

we find there is no any systematic variation of rotational velocity with metallicity. That indicates the independence of rotational velocity with metallicity.

Metallicity [Fe/H]	All	$-0.9 < [\text{Fe}/\text{H}] < -0.5$	$-1.3 < [\text{Fe}/\text{H}] < -0.9$	$-2.5 < [\text{Fe}/\text{H}] < -1.3$
f_1	$0.650^{+0.042}_{-0.041}$	$0.678^{+0.056}_{-0.049}$	$0.706^{+0.06}_{-0.06}$	$0.611^{+0.073}_{-0.091}$
f_2	$0.121^{+0.05}_{-0.03}$	$0.253^{+0.046}_{-0.063}$	$0.130^{+0.049}_{-0.040}$	$0.094^{+0.045}_{-0.023}$
f_3	0.229	0.069	0.164	0.295
$V_{T,1}$	-5^{+3}_{-3}	2^{+4}_{-1}	-10^{+4}_{-4}	-17^{+5}_{-5}
$\sigma_{T,1}$	55^{+3}_{-3}	49^{+4}_{-3}	61^{+4}_{-4}	62^{+6}_{-6}
$V_{T,2}$	135^{+14}_{-20}	114^{+20}_{-10}	138^{+25}_{-25}	151^{+8}_{-32}
$\sigma_{T,2}$	59^{+13}_{-12}	71^{+8}_{-10}	72^{+11}_{-12}	47^{+31}_{-23}
$V_{T,3}$	-41^{+15}_{-19}	-29^{+24}_{-64}	-94^{+40}_{-49}	-56^{+18}_{-26}
$\sigma_{T,3}$	153^{+7}_{-7}	138^{+23}_{-30}	148^{+15}_{-15}	157^{+13}_{-12}
Number	3081	1181	1039	861

Table 4.2: Table shows the results of MCMC simulation for different K-giant stars grouping that we made.

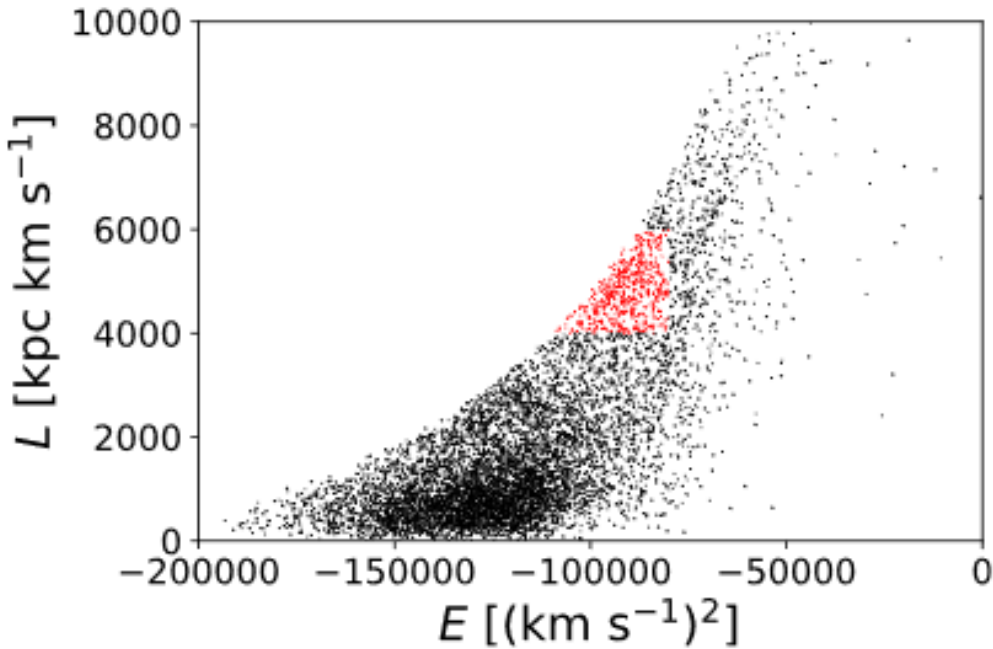


Figure 4.16: Energy versus angular momentum plot obtained by Bird *et al.* (2018) [8]

Fig. 4.16 shows the energy versus the angular momentum plot obtained by Bird *et al.* (2018) [8] for K-giant stars. In this plot, we can observe the dense region on the bottom that represents the halo and the red part represents the presence of the Sagittarius substructure.

When comparing our results to Bird *et al.* (2018), it must be pointed out that the grey point at the bottom of the plot in Fig. (4.7) represents the stellar halo. It should be noted that the majority of our K-giant stars is in the halo region.

Chapter 5

Conclusions & Future Works

5.1 Conclusion

GALAH DR3 was crossmatched with Gaia EDR3 to obtain the full 6 – dimensional phase space information. We derived the rotational velocity, velocity anisotropy and energy as well as momentum of K-giant halo stars based on astrometry and photometric as well as spectroscopic parameters from both Gaia and GALAH surveys. We have used radial velocity, proper motions and parallax from Gaia and metallicities, logg, and effective surface temperature from GALAH. We also observed the relationship between the effect of metallicity on rotational velocity and carefully analyzed the metallicity effects on rotational velocity. On the basis of our results, we have reached out the following conclusions;

- We found the rotational velocity of inner halo to be $V_T = -5^{+3}_{-3}$ km s⁻¹ which is quite similar to the result observed by Kordopatis *et al.* (2013) [29], Carollo *et al.* (2010) [27]. This also supports the fact that the inner halo of the Milky Way is nearly stationary.
- We obtained rotational velocity of the metal-poor thick disk, $V_T = 135^{+14}_{-20}$ km s⁻¹ which is in complete agreement with the result obtained by the Kordopatis *et al.* (2013) [29], Carollo *et al.* (2010) [27] for MWTD.

- Third component that we obtained in our sample is of outer halo which displays the large retrograde motion, $V_T = -41^{+15}_{-19} \text{ Km s}^{-1}$, this result is in close agreement with a rotational velocity of outer halo determined by the Carollo *et al.* (2007) [30].
- On analyzing the correlation of metallicity with rotational velocity, we didn't find the significant variation of rotational velocity with metallicity which is similar to the result obtained by Tian *et al.* (2019) [6] and Kafle *et al.* (2017) [7] also didn't find a significant variation of rotational velocity with metallicity for K-giant.
- We considered the entire sample to be one and then determined the velocity anisotropy $\beta = 0.48$ which suggests K-giants has radially biased orbit.
- We studied the variation of the β with the galactocentric radius, we found they incline toward tangential orbit as distance increases which is similar to the result obtained by the Kafle *et al.* [31].
- We studied the variation of the β with metallicity and found no significant deviation in value of β for different metallicity range which is similar to the result obtained by Kafle *et al.* [7].

5.2 Future Works

In future, we intend to determine the error of velocity anisotropy. We are aiming to expand the horizon of our study by performing a similar analysis for other types of stars like MSTOs and BHBs. We are also aiming to expand the sample size by the inclusion of stars beyond 4 kpc and metal rich stars. We are planning to work with LAMOST data as soon as they will release their new data publicly.

References

- [1] H. Karttunen, P. Kroger, H. Oja, M. Putanen, K.J. Donner, *Fundamental Astronomy* (Springer Berlin Heidelberg, 2007).
- [2] A. Helmi, The Formation of the Galactic Halo, Leiden University, Leiden, Netherlands, (2000).
- [3] E.F. del Peloso, L. da Silva, G.F.P. de Mello, L.I. Arany-Prado, Proc Int Astron Union, **1**, 485 - 486, (2005).
- [4] T. Bensby, A. Alves-Brito, M. Oey , D. Yong, J. Mel'endez, ApJ, **735**, L46, (2011).
- [5] M. Martig, I. Minchev, M. Ness, M. Fouesneau, H.W. Rix, ApJ, **831**, 139, (2016).
- [6] H. Tian, C. Liu, Y. Xu, X. Xue, ApJ, **871**, 184, (2019).
- [7] P. R. Kafle, S. Sharma, A. S. G. Robotham, R. K. Pradhan, M. Guglielmo, L. J. M. Davies, S. P. Driver, RAS, **470**, 2959–2971, (2017).
- [8] S. A. Bird, X. X. Xue, C. Liu, J. Shen, C. Flynn, C. Yang, **157**, 104, (2019).
- [9] T. Koupelis, *In Quest of the Universe* (Jones & Bartlett Publishers, 2012).

- [10] J. Binney, Mon. Notices Royal Astron. Soc., **190**, 873-880, (1980).
- [11] <http://astro.utoronto.ca/~bovy/>
- [12] F. Matteucci, *The Chemical Evolution of the Galaxy* (Springer-Verlag Berlin Heidelberg, 2001).
- [13] R. N. Mantegna, H. E. Stanley, *An Introduction To Econophysics Correlations And Complexity In Finance* (Cambridge University Press, 2004).
- [14] D. Hogg, D. Foreman-Mackey, astro-ph.IM, **236**, 11, (2018).
- [15] P. J. McMillian, MNRAS, **465**, 76 - 94, (2017).
- [16] <https://www.cosmos.esa.int/web/gaia/science-performance>
- [17] S. Jordan, Astron. Nachr, **329**, 875 - 880, (2008).
- [18] <https://galah-survey.org/>
- [19] Gaia Collaboration *et al.*, arXiv preprint (arXiv:2012.01533), (2020).
- [20] S. Buder *et al.*, arXiv preprint (arXiv:2011.02505), (2020).
- [21] C. Liu *et al.*, ApJ, **790**, 110, (2014).

- [22] J. Bland-Hawthorn, O. Gerhard, ARA&A, **54**, 529 - 596, (2016).
- [23] R. Schönrich, J. Binney, W. Dehnen, MNRAS, **403**, 1829 - 1833, (2010).
- [24] D. R. H. Johnson, D. R. Soderblom, AJ, **93**, 864, (1987).
- [25] A. G. A. Brown, H. M. Velazquez, L. A. Aguilar, MNRAS, **359**, 1287 – 1305, (2005).
- [26] J. Bovy, ApJS, **216**, 29, (2015).
- [27] D. Carolla, T.C. Beers, M. Chiba, J.E. Norris, K.C. Lee, Y.S. Lee, Z. Ivezic, C.M. Rockosi, B. Yang, ApJ, **712**, 692 - 727, (2010).
- [28] D. Foreman-Mackey, D.W. Hogg, D. Lang, J. Goodman, Publ. Astron. Soc. Pac., **125**, 306, (2013).
- [29] G. Kordopatis et al., MNRAS, **436**, 3231 - 3246, (2013).
- [30] D. carolla et al., Nature, **450**, 1020 – 1025, (2007).
- [31] P. R. Kafle, S. Sharma, G. F. Lewis, J. Bland-Hawthorn, MNRAS, **430**, 2973 - 2978, (2013).
- [32] A. J. Deason, V. Belokurov, N. W. Evans, MNRAS, **411**, 1480 - 1494, (2011).